

ON COURANT'S NODAL DOMAIN PROPERTY FOR LINEAR COMBINATIONS OF EIGENFUNCTIONS PART II

PIERRE BÉRARD AND BERNARD HELFFER

To Erik Balslev, in memoriam

ABSTRACT. Generalizing Courant's nodal domain theorem, the "Extended Courant property" is the statement that a linear combination of the first n eigenfunctions has at most n nodal domains. In a previous paper (Documenta Mathematica, 2018, Vol. 23, pp. 1561–1585), we gave simple counterexamples to this property, including convex domains. In the present paper, using some input from numerical computations, we pursue the investigation of the Extended Courant property with two new examples, the equilateral rhombus and the regular hexagon.

1. INTRODUCTION

1.1. Notation. Let $\Omega \subset \mathbb{R}^2$ be a piecewise smooth bounded open domain (we will actually only work with convex polygonal domains), with boundary $\partial\Omega = \overline{\Gamma_1} \sqcup \overline{\Gamma_2}$, where Γ_1, Γ_2 are two disjoint open subsets of $\partial\Omega$. We consider the eigenvalue problem

$$(1.1) \quad \begin{cases} -\Delta u = \mu u & \text{in } \Omega, \\ u = 0 & \text{on } \Gamma_1, \\ \nu \cdot u = 0 & \text{on } \Gamma_2, \end{cases}$$

where ν is the outer unit normal along $\partial\Omega$ (defined almost everywhere).

Let $\{\mu_i(\Omega, \mathbf{dn}), i \geq 1\}$ (resp. $\text{sp}(\Omega, \mathbf{dn})$) denote the eigenvalues (resp. the spectrum) of problem (1.1). We always list the eigenvalues in non-decreasing order, with multiplicities, starting with the index 1. We simply write μ_i , and skip mentioning the domain Ω , or the boundary condition \mathbf{dn} , whenever the context is clear. Examples of eigenvalue problems with mixed boundary conditions appear in Sections 2 and 3.

Date: February 2, 2022 (berard-helffer-ecp-II-balslev-190926-ha.tex).

2010 Mathematics Subject Classification. 35P99, 35Q99, 58J50.

Key words and phrases. Eigenfunction, Nodal domain, Courant nodal domain theorem.

The authors express their hearty thanks to V. Bonnaillie-Noël for providing numerical simulations at an earlier stage of their research.

Let $\mathcal{E}(\mu)$ denote the eigenspace associated with the eigenvalue μ .

Define the *min-index* $\kappa(\mu)$ of the eigenvalue μ as

$$(1.2) \quad \kappa(\mu) = \min \{m \mid \mu = \mu_m\} .$$

1.2. Courant's nodal domain theorem. Let ϕ be an eigenfunction of (1.1). The *nodal set* $\mathcal{Z}(\phi)$ of ϕ is defined as the closure of the set of (interior) zeros of ϕ ,

$$(1.3) \quad \mathcal{Z}(\phi) := \overline{\{x \in \Omega \mid \phi(x) = 0\}} .$$

A *nodal domain* of ϕ is a connected component of the set $\Omega \setminus \mathcal{Z}(\phi)$. Call $\beta_0(\phi)$ the number of nodal domains of ϕ . We recall the following classical theorem, [12, Chap. VI.6].

Theorem 1.1 (Courant, 1923). *Assume that the eigenvalues of (1.1) are listed in non-decreasing order, with multiplicities,*

$$(1.4) \quad \mu_1 < \mu_2 \leq \mu_3 \leq \cdots .$$

Then, for any eigenfunction $\phi \in \mathcal{E}(\mu)$ of (1.1), associated with the eigenvalue μ ,

$$(1.5) \quad \beta_0(\phi) \leq \kappa(\mu) .$$

In particular, any $\phi \in \mathcal{E}(\mu_k)$ has at most k nodal domains,

Courant's theorem is a partial generalization, to higher dimensions, of a classical theorem of C. Sturm (1836). Indeed, in dimension 1, a k -th eigenfunction of the Sturm-Liouville operator $-\frac{d^2}{dx^2} + q(x)$ in $]a, b[$, with Dirichlet, Neumann, or mixed Dirichlet-Neumann boundary condition at $\{a, b\}$, has exactly k nodal domains in $]a, b[$. In dimension 2 (or higher), Courant's theorem is not sharp. On the one hand, A. Stern (1925) proved that for the square with Dirichlet boundary condition, or for the 2-sphere, there exist eigenfunctions of arbitrarily high energy, with exactly two or three nodal domains. On the other hand, Å. Pleijel (1956) proved that, for any bounded domain in \mathbb{R}^2 , there are only finitely many Dirichlet eigenvalues for which Courant's theorem is sharp. We refer to [7, 24] for more details, and to [20] for Pleijel's estimate under Neumann boundary condition.

Another remarkable theorem of Sturm states that any non trivial linear combination $u = \sum_{k=m}^n a_j u_j$ of eigenfunctions of the operator $-\frac{d^2}{dx^2} + q(x)$ has at most $(n - 1)$ zeros (counted with multiplicities), and at least $(m - 1)$ sign changes in the interval $]a, b[$, see [10].

A footnote in [12, p. 454] states that Courant's theorem *may be generalized as follows: Any linear combination of the first n eigenfunctions divides the domain, by means of its nodes, into no more than n subdomains. See the Göttingen dissertation of H. Herrmann, Beiträge zur Theorie der Eigenwerten und Eigenfunktionen, 1932.*

For later reference, we introduce the following definition.

Definition 1.2. *We say that the Extended Courant property is true for the eigenvalue problem (Ω, \mathbf{b}) , or simply that the $\text{ECP}(\Omega, \mathbf{b})$ is true, if, for any $m \geq 1$, and for any linear combination $v = \sum_{\mu_j \leq \mu_m} u_{\mu_j}$, with $u_{\mu_j} \in \mathcal{E}(\mu_j(\Omega, \mathbf{b}))$,*

$$(1.6) \quad \beta_0(v) \leq \kappa(\mu_m) \leq m.$$

The footnote statement in the book of Courant and Hilbert, amounts to saying that $\text{ECP}(\Omega)$ is true for any bounded domain. Already in 1956, Pleijel [24, p. 550] mentioned that he could not find a proof of this statement in the literature. In 1973, V. Arnold [2, 4] related the statement in Courant-Hilbert to Hilbert's 16th problem. Indeed, should $\text{ECP}(\mathbb{R}P^N, g_0)$ be true (where g_0 is the usual metric), then the complement of any algebraic hypersurface of degree n in $\mathbb{R}P^N$ would have at most $\binom{N}{N+n-2} + 1$ connected components. Arnold pointed out that while $\text{ECP}(\mathbb{R}P^2, g_0)$ is indeed true, $\text{ECP}(\mathbb{R}P^3, g_0)$ is false due to counterexamples produced by O. Viro [26]. More recently, Gladwell and Zhu [14, p. 276] remarked that Herrmann in his dissertation and subsequent publications *had not even stated, let alone proved* the ECP. They also produced some numerical evidence that the ECP is false for non-convex domains in \mathbb{R}^2 with the Dirichlet boundary condition, and conjectured that it is true for convex domains.

Our motivations to look into the Extended Courant property came from reading the papers [3, 14, 18]. In [9], we gave simple counterexamples to the ECP for domains with the Dirichlet or the Neumann boundary conditions (equilateral triangle, hypercubes, domains and surfaces with cracks). This was made possible by the fact that the eigenvalues and eigenfunctions of these domains are known explicitly. In [11], we proved that $\text{ECP}(\Omega, \mathbf{n})$ is false for a continuous family of smooth convex domains in \mathbb{R}^2 , with the symmetries of, and close to the equilateral triangle.

In the present paper, we continue our investigations of the Extended Courant property by studying two examples, the equilateral rhombus $\mathcal{R}h_e$ and the regular hexagon \mathcal{H} , which are related to the equilateral triangle. The eigenvalues and eigenfunctions of these domains are not known explicitly (except for a small subset of them). Using the symmetries of these domains, and some input from numerical computations, we are able to describe the nodal patterns of the first eigenfunctions, and conclude that the equilateral rhombus and the regular hexagon provide counterexamples to the ECP.

The paper is organized as follows. In Section 2, we analyze the structure of the first eigenvalues and eigenfunctions of the equilateral rhombus $\mathcal{R}h_e$ with either the Neumann or the Dirichlet boundary condition. Subsections 2.1, 2.2 and 2.3 provide technical ideas which are used in

Section 3 as well. In Subsection 2.5, we prove that $\text{ECP}(\mathcal{R}h_e, \mathfrak{n})$ is false. In Subsection 2.7, we give numerical evidence that $\text{ECP}(\mathcal{R}h_e, \mathfrak{d})$ is false as well. In Section 3, we analyze the structure of the first eigenvalues and eigenfunctions of the regular hexagon \mathcal{H} with either the Neumann or the Dirichlet boundary condition. In Subsection 3.4, we give numerical evidence that $\text{ECP}(\mathcal{H}, \mathfrak{d})$ is false. In Subsection 3.6, we give numerical evidence that $\text{ECP}(\mathcal{H}, \mathfrak{n})$ is false. In Section 4, we explain our numerical approach, and we make some final remarks and conjectures.

2. THE EQUILATERAL RHOMBUS

2.1. Symmetries and spectra. In this subsection, we analyze how symmetries influence the structure of the eigenvalues and eigenfunctions. The analysis is carried out for the equilateral rhombus, but the basics ideas work for the regular hexagon as well, and will be used in Section 3.

In the sequel, we denote by the same letter L a line in \mathbb{R}^2 , and the mirror symmetry with respect to this line. We denote by L^* the action of the symmetry L on functions, $L^*\phi = \phi \circ L$.

A function ϕ is *even* (or *invariant*) with respect to L if $L^*\phi = \phi$. It is *odd* (or *anti-invariant*) with respect to L if $L^*\phi = -\phi$. In the former case, the line L is an *anti-nodal* line for ϕ , i.e., the normal derivative $\nu_L \cdot \phi$ is zero along L , where ν_L denotes a unit field normal to L along L . In the latter case, the line L is a *nodal* line for ϕ , i.e., ϕ vanishes along L .

Let $\mathcal{R}h_e$ be the interior of the equilateral rhombus with sides of length 1, and vertices $(-\frac{\sqrt{3}}{2}, 0)$, $(0, -\frac{1}{2})$, $(\frac{\sqrt{3}}{2}, 0)$ and $(0, \frac{1}{2})$. Call D and M its diagonals (resp. the longer one and the shorter one). The diagonal M divides the rhombus into two equilateral triangles. The diagonals D and M divide the rhombus into four hemiequilateral triangles. In the sequel, we use the generic notation \mathcal{T}_e (resp. \mathcal{T}_h) for any of the equilateral triangles (resp. hemiequilateral triangles) into which the rhombus decomposes, see Figure 2.1.

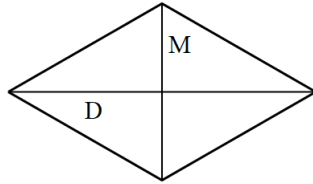


FIGURE 2.1. The equilateral rhombus $\mathcal{R}h_e$, and its diagonals

For $L \in \{D, M\}$, define the sets

$$(2.1) \quad \begin{cases} \mathcal{S}_{L,+} &= \{\phi \in L^2(\mathcal{R}h_e) \mid L^*\phi = +\phi\}, \\ \mathcal{S}_{L,-} &= \{\phi \in L^2(\mathcal{R}h_e) \mid L^*\phi = -\phi\}. \end{cases}$$

Then, we have the orthogonal decomposition,

$$(2.2) \quad L^2(\mathcal{R}h_e) = \mathcal{S}_{L,+} \overset{\perp}{\oplus} \mathcal{S}_{L,-},$$

with respect to the L^2 -inner product. Indeed, any $\phi \in L^2(\mathcal{R}h_e)$ can be decomposed as

$$(2.3) \quad \phi = \frac{1}{2}(I + L^*)\phi + \frac{1}{2}(I - L^*)\phi,$$

where I denotes the identity map.

The symmetries D and M commute

$$(2.4) \quad M \circ D = D \circ M = R_\pi,$$

where R_θ denotes the rotation with center 0 (the center of the rhombus), and angle θ . It follows that D^* leaves the subspaces $\mathcal{S}_{M,\pm}$ globally invariant, and that M^* leaves the subspaces $\mathcal{S}_{D,\pm}$ globally invariant. As a consequence, we have the orthogonal decomposition,

$$(2.5) \quad L^2(\mathcal{R}h_e) = \mathcal{S}_{+,+} \overset{\perp}{\oplus} \mathcal{S}_{-,-} \overset{\perp}{\oplus} \mathcal{S}_{+,-} \overset{\perp}{\oplus} \mathcal{S}_{-,+},$$

where

$$(2.6) \quad \mathcal{S}_{\sigma,\tau} := \{\phi \in L^2(\mathcal{R}h_e) \mid D^*\phi = \sigma\phi \text{ and } M^*\phi = \tau\phi\},$$

for $\sigma, \tau \in \{+, -\}$.

Similar decompositions hold for $H^1(\mathcal{R}h_e)$ and $H_0^1(\mathcal{R}h_e)$, the Sobolev spaces which are used in the variational presentation of the Neumann (resp. Dirichlet) eigenvalue problem for the rhombus.

In the following figures, anti-nodal lines are indicated by dashed lines, and nodal lines by solid lines. Figure 3.2 displays the nodal and anti-nodal lines common to all functions in $H^1(\mathcal{R}h_e) \cap \mathcal{S}_{\sigma,\tau}$, where $\sigma, \tau \in \{+, -\}$.

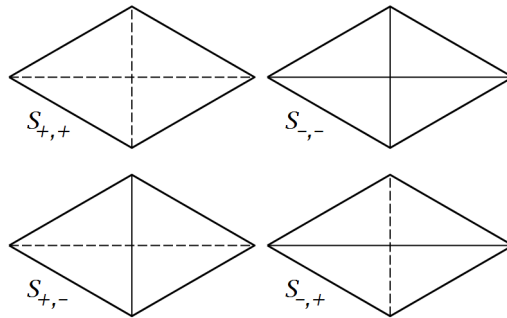


FIGURE 2.2. Spaces $\mathcal{S}_{\sigma,\tau}$ for $\mathcal{R}h_e$

Because the Laplacian commutes with the isometries D and M , the above orthogonal decompositions descend to each eigenspace of $-\Delta$ for $\mathcal{R}h_e$, with the boundary condition $\mathbf{b} \in \{\mathfrak{d}, \mathfrak{n}\}$ on $\partial\mathcal{R}h_e$. The eigenfunctions in each summand correspond to eigenfunctions of $-\Delta$ for the equilateral triangle (decomposition (2.2) with $L = M$), or for the hemiequilateral triangle (decomposition (2.6)), with the boundary condition \mathbf{b} on the side supported by $\partial\mathcal{R}h_e$, and with mixed boundary conditions, either Dirichlet or Neumann, on the sides supported by the diagonals.

To be more explicit, we need naming the eigenvalues as in Subsection 1.1. For this purpose, we partition the boundaries of \mathcal{T}_e and \mathcal{T}_h into their three sides. For \mathcal{T}_h , we number the sides 1, 2, 3, in decreasing order of length, see Figure 2.3. For example, $\mu_i(\mathcal{T}_h, \mathfrak{n}\mathfrak{d}\mathfrak{n})$ denotes the i -th eigenvalue of $-\Delta$ in \mathcal{T}_h with Neumann boundary condition on the longest (1) and shortest (3) sides, and Dirichlet boundary condition on the other side (2).

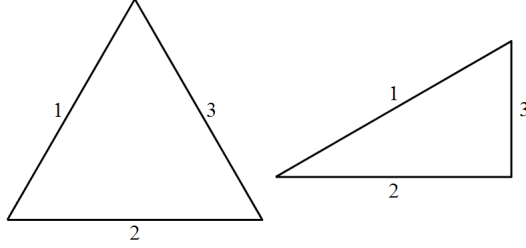


FIGURE 2.3. Labelling the sides of \mathcal{T}_e and \mathcal{T}_h

2.2. Riemann-Schwarz reflection principle. In this subsection, we recall the “Riemann-Schwarz reflection principle” which we will use repeatedly in the sequel.

Consider the decomposition $\mathcal{R}h_e = \mathcal{T}_{e,1} \sqcup \mathcal{T}_{e,2}$, with $M(\mathcal{T}_{e,1}) = \mathcal{T}_{e,2}$. Choose a boundary condition $\mathbf{a} \in \{\mathfrak{d}, \mathfrak{n}\}$ on $\partial\mathcal{R}h_e$. Given an eigenvalue λ of $-\Delta$ for $(\mathcal{R}h_e, \mathbf{a})$, and $\sigma \in \{+, -\}$, consider the subspace $\mathcal{E}(\lambda) \cap \mathcal{S}_{M,\sigma}$ of eigenfunctions $\phi \in \mathcal{E}(\lambda)$ such that $M^*\phi = \sigma\phi$.

If $0 \neq \phi \in \mathcal{E}(\lambda) \cap \mathcal{S}_{M,\sigma}$, then $\phi|_{\mathcal{T}_{e,1}}$ is an eigenfunction of $-\Delta$ for $(\mathcal{T}_{e,1}, \mathbf{a}\mathbf{a}\mathbf{b})$, with $\mathbf{b} = \mathfrak{n}$ if $\sigma = +$, and $\mathbf{b} = \mathfrak{d}$ if $\sigma = -$, associated with the same eigenvalue λ .

Conversely, let ψ be an eigenfunction of $(\mathcal{T}_{e,1}, \mathbf{a}\mathbf{a}\mathbf{b})$, with eigenvalue $\mu_m(\mathcal{T}_{e,1}, \mathbf{a}\mathbf{a}\mathbf{b})$, for some $m \geq 1$. Define the function $\check{\psi}$ on $\mathcal{R}h_e$ such that $\check{\psi}|_{\mathcal{T}_{e,1}} = \psi$ and $\check{\psi}|_{\mathcal{T}_{e,2}} = \sigma\psi \circ M$. This means that $\check{\psi}$ is obtained by extending ψ across M to $\mathcal{T}_{e,2}$ by symmetry, in such a way that $M^*\check{\psi} = \sigma\check{\psi}$. It is easy to see that the function $\check{\psi}$ is an eigenfunction of

$-\Delta$ for $(\mathcal{R}h_e, \mathbf{a})$ (in particular it is smooth in a neighborhood of M), with eigenvalue $\mu_m(\mathcal{T}_{e,1}, \mathbf{aab})$, so that $\check{\psi} \in \mathcal{E}(\mu_m) \cap \mathcal{S}_{M,\sigma}$.

The above considerations prove the first two assertions in the following proposition. The proof of the third and fourth assertions is similar, using the symmetries D and M , and the decomposition of $\mathcal{R}h_e$ into hemiequilateral triangles $\mathcal{T}_{h,j}$, $1 \leq j \leq 4$.

Proposition 2.1 (Reflection principle). *For any $\mathbf{a} \in \{\mathfrak{d}, \mathfrak{n}\}$ and any $\lambda \in \text{sp}(\mathcal{R}h_e, \mathbf{a})$,*

- (i) $\mathcal{E}(\lambda, (\mathcal{R}h_e, \mathbf{a})) \cap \mathcal{S}_{M,+} \neq \{0\}$ if and only if $\lambda \in \text{sp}(\mathcal{T}_e, \mathbf{aan})$, and the map $\phi \mapsto \phi|_{\mathcal{T}_{e,1}}$ is a bijection from $\mathcal{E}(\lambda, (\mathcal{R}h_e, \mathbf{a})) \cap \mathcal{S}_{M,+}$ onto $\mathcal{E}(\lambda, (\mathcal{T}_e, \mathbf{aan}))$;
- (ii) $\mathcal{E}(\lambda, (\mathcal{R}h_e, \mathbf{a})) \cap \mathcal{S}_{M,-} \neq \{0\}$ if and only if $\lambda \in \text{sp}(\mathcal{T}_e, \mathbf{aad})$, and the map $\phi \mapsto \phi|_{\mathcal{T}_{e,1}}$ is a bijection from $\mathcal{E}(\lambda, (\mathcal{R}h_e, \mathbf{a})) \cap \mathcal{S}_{M,-}$ onto $\mathcal{E}(\lambda, (\mathcal{T}_e, \mathbf{aad}))$.

More generally, define $\epsilon(\mathfrak{n}) = +$ and $\epsilon(\mathfrak{d}) = -$. Then, for any $\lambda \in \text{sp}(\mathcal{R}h_e, \mathbf{a})$, and any $\mathbf{b}, \mathbf{c} \in \{\mathfrak{d}, \mathfrak{n}\}$,

- (iii) $\mathcal{E}(\lambda, (\mathcal{R}h_e, \mathbf{a})) \cap \mathcal{S}_{\epsilon(\mathbf{b}), \epsilon(\mathbf{c})} \neq \{0\}$ if and only if $\lambda \in \text{sp}(\mathcal{T}_h, \mathbf{abc})$, and the map $\phi \mapsto \phi|_{\mathcal{T}_{h,1}}$ is a bijection from $\mathcal{E}(\lambda, (\mathcal{R}h_e, \mathbf{a})) \cap \mathcal{S}_{\epsilon(\mathbf{b}), \epsilon(\mathbf{c})}$ onto $\mathcal{E}(\lambda, (\mathcal{T}_h, \mathbf{abc}))$.

Furthermore, the multiplicity of the number λ as eigenvalue of $(\mathcal{R}h_e, \mathbf{a})$ is the sum, over $\mathbf{b}, \mathbf{c} \in \{\mathfrak{d}, \mathfrak{n}\}$, of the multiplicities of λ as eigenvalue of $(\mathcal{T}_h, \mathbf{abc})$ (with the convention that the multiplicity is zero if λ is not an eigenvalue).

2.3. Some useful results. In this subsection, we recall some known results for the reader's convenience.

2.3.1. Eigenvalue inequalities. The following proposition is a particular case of a result of V. Lotoreichik and J. Rohleder.

Proposition 2.2 ([22], Proposition 2.3). *Let $\Omega \subset \mathbb{R}^2$ be a polygonal bounded domain whose boundary is decomposed as $\partial\Omega = \overline{\Gamma_1} \sqcup \overline{\Gamma_2} \sqcup \overline{\Gamma_3}$, where the Γ_i 's are non-empty open subsets of $\partial\Omega$. Consider the eigenvalue problems for $-\Delta$ in Ω , with the boundary condition $\mathbf{b}_i \in \{\mathfrak{d}, \mathfrak{n}\}$ on Γ_i , and list the eigenvalues $\mu_j(\Omega, \mathbf{b}_1 \mathbf{b}_2 \mathbf{b}_3)$ in non-decreasing order, with multiplicities, starting from the index 1.*

Then, for any $j \geq 1$, the following strict inequalities hold.

$$(2.7) \quad \begin{cases} \mu_j(\Omega, \mathbf{nnn}) < \mu_j(\Omega, \mathbf{ndn}) < \mu_j(\Omega, \mathbf{ndd}), \\ \mu_j(\Omega, \mathbf{nnn}) < \mu_j(\Omega, \mathbf{nnn}) < \mu_j(\Omega, \mathbf{ndd}), \end{cases}$$

and

$$(2.8) \quad \begin{cases} \mu_i(\mathcal{T}_h, \mathbf{dnn}) < \mu_i(\mathcal{T}_h, \mathbf{ddn}) < \mu_i(\mathcal{T}_h, \mathbf{ddd}), \\ \mu_i(\mathcal{T}_h, \mathbf{dnn}) < \mu_i(\mathcal{T}_h, \mathbf{dnd}) < \mu_i(\mathcal{T}_h, \mathbf{ddd}). \end{cases}$$

The preceding inequalities can in particular be applied to the triangle \mathcal{T}_h . In this particular case, when $j = 1$, we have the following more precise inequalities which are due to B. Siudeja.

Proposition 2.3 ([25], Theorem 1.1). *The eigenvalues of \mathcal{T}_h with mixed boundary conditions are denoted by $\mu_i(\mathbf{abc})$, with the sides listed in decreasing order of length. They satisfy the following inequalities.*

$$\begin{aligned} 0 = \mu_1(\mathbf{nnn}) &< \mu_1(\mathbf{nn}\partial) < \mu_1(\mathbf{n}\partial\mathbf{n}) = \mu_2(\mathbf{nnn}) < \mu_1(\partial\mathbf{nn}) \cdots \\ &\cdots < \mu_1(\mathbf{n}\partial\partial) < \mu_1(\partial\mathbf{n}\partial) < \mu_1(\partial\partial\mathbf{n}) < \mu_1(\partial\partial\partial). \end{aligned}$$

Remark 2.4. *We do not know whether there are any general inequalities between the eigenvalues $\mu_i(\mathcal{T}_h, \mathbf{n}\partial\mathbf{n})$ and $\mu_i(\mathcal{T}_h, \mathbf{nn}\partial)$, or between the eigenvalues $\mu_i(\mathcal{T}_h, \partial\partial\mathbf{n})$ and $\mu_i(\mathcal{T}_h, \partial\mathbf{n}\partial)$, for $i \geq 2$.*

2.3.2. *Eigenvalues of some mixed boundary value problems for \mathcal{T}_h .* For later reference, we describe the eigenvalues of four mixed eigenvalue problems for \mathcal{T}_h . This description follows easily from [8] or [9, Appendix A].

The eigenvalues of the equilateral triangle \mathcal{T}_e , with either the Dirichlet or the Neumann boundary condition on $\partial\mathcal{T}_e$, are the numbers

$$(2.9) \quad \hat{\lambda}(m, n) = \frac{16\pi^2}{9} (m^2 + mn + n^2),$$

with $(m, n) \in \mathbb{N} \times \mathbb{N}$ for the Neumann boundary condition, and $(m, n) \in \mathbb{N}^\bullet \times \mathbb{N}^\bullet$ for the Dirichlet boundary condition (here $\mathbb{N}^\bullet = \mathbb{N} \setminus \{0\}$). The multiplicities are given by,

$$(2.10) \quad \text{mult}(\hat{\lambda}_0) = \# \left\{ (m, n) \in \mathcal{L} \mid \hat{\lambda}(m, n) = \hat{\lambda}_0 \right\},$$

with $\mathcal{L} = \mathbb{N} \times \mathbb{N}$ for the Neumann boundary condition, and $\mathcal{L} = \mathbb{N}^\bullet \times \mathbb{N}^\bullet$ for the Dirichlet boundary condition.

One can associate one or two real eigenfunctions with such a pair (m, n) . When $m = n$, there is only one associated eigenfunction, and it is D -invariant (here D denotes the bisector of one side of \mathcal{T}_e , see Figure 2.1). When $m \neq n$, there are two associated eigenfunctions, one invariant with respect to D , the other one anti-invariant. As a consequence, one can explicitly describe the eigenvalues and eigenfunctions of the four eigenvalue problems $(\mathcal{T}_h, \mathbf{nnn})$, $(\mathcal{T}_h, \mathbf{n}\partial\mathbf{n})$ (they arise from the Neumann problem for \mathcal{T}_e), and $(\mathcal{T}_h, \partial\mathbf{n}\partial)$, $(\mathcal{T}_h, \partial\partial\partial)$ (they arise from the Dirichlet problem for \mathcal{T}_e).

The resulting eigenvalues are given in Table 2.1.

Remark 2.5. *As far as we know, there are no such explicit formulas for the eigenvalues of the other mixed boundary value problems for \mathcal{T}_h .*

TABLE 2.1. Four mixed eigenvalue problems for \mathcal{T}_h

Eigenvalue problem	Eigenvalues
$(\mathcal{T}_h, \mathbf{nnn})$	$\hat{\lambda}(m, n)$, for $0 \leq m \leq n$
$(\mathcal{T}_h, \mathbf{n\partial n})$	$\hat{\lambda}(m, n)$, for $0 \leq m < n$
$(\mathcal{T}_h, \mathbf{\partial n \partial})$	$\hat{\lambda}(m, n)$, for $1 \leq m \leq n$
$(\mathcal{T}_h, \mathbf{\partial \partial \partial})$	$\hat{\lambda}(m, n)$, for $1 \leq m < n$

TABLE 2.2. First eigenvalues for $(\mathcal{T}_h, \mathbf{nnn})$ and $(\mathcal{T}_h, \mathbf{n\partial n})$

Eigenvalue	Pairs	$(\mathcal{T}_h, \mathbf{nnn})$	$(\mathcal{T}_h, \mathbf{n\partial n})$
0	(0, 0)	μ_1	
$\frac{16\pi^2}{9}$	(0, 1), (1, 0)	μ_2	μ_1
$3 \times \frac{16\pi^2}{9}$	(1, 1)	μ_3	
$4 \times \frac{16\pi^2}{9}$	(0, 2), (2, 0)	μ_4	μ_2
$7 \times \frac{16\pi^2}{9}$	(1, 2), (2, 1)	μ_5	μ_3
$9 \times \frac{16\pi^2}{9}$	(0, 3), (3, 0)	μ_6	μ_4

TABLE 2.3. First eigenvalues for $(\mathcal{T}_h, \mathbf{\partial n \partial})$ and $(\mathcal{T}_h, \mathbf{\partial \partial \partial})$

Eigenvalue	Pairs	$(\mathcal{T}_h, \mathbf{\partial n \partial})$	$(\mathcal{T}_h, \mathbf{\partial \partial \partial})$
$3 \times \frac{16\pi^2}{9}$	(1, 1)	μ_1	
$7 \times \frac{16\pi^2}{9}$	(1, 2), (2, 1)	μ_2	μ_1
$12 \times \frac{16\pi^2}{9}$	(2, 2)	μ_3	
$13 \times \frac{16\pi^2}{9}$	(1, 3), (3, 1)	μ_4	μ_2
$19 \times \frac{16\pi^2}{9}$	(2, 3), (3, 2)	μ_5	μ_3
$21 \times \frac{16\pi^2}{9}$	(1, 4), (4, 1)	μ_6	μ_4

Tables 2.1–2.3 display the first few eigenvalues, the corresponding pairs of integers, and the corresponding indexed eigenvalues for the given mixed boundary value problems for \mathcal{T}_h .

Remark 2.6. For later reference, we point out that the eigenvalues which appear in Tables 2.2 and 2.3 are simple.

2.4. Rhombus with Neumann boundary condition. In this subsection, we choose the Neumann boundary condition on the boundary $\partial\mathcal{R}h_e$ of the equilateral rhombus.

2.4.1. The first Neumann eigenvalues of $\mathcal{R}h_e$.

Proposition 2.7. Let ν_i denote the eigenvalues of $(\mathcal{R}h_e, \mathbf{n})$. Then,

$$(2.11) \quad 0 = \nu_1 < \nu_2 < \nu_3 = \nu_4 < \nu_5 \leq \dots$$

More precisely,

(i) The second eigenvalue ν_2 is simple and satisfies

$$(2.12) \quad \nu_2 = \mu_1(\mathcal{T}_h, \mathbf{nn}\mathfrak{d}) = \mu_1(\mathcal{T}_e, \mathbf{nn}\mathfrak{d}).$$

If $u_2 \in \mathcal{E}(\nu_2)$, then it is invariant under the symmetry D , anti-invariant under the symmetry M , and $\mathcal{Z}(u_2) = M \cap \mathcal{R}h_e$.

Furthermore, $u_2|_{\mathcal{T}_h}$ is a first eigenfunction of $(\mathcal{T}_h, \mathbf{nn}\mathfrak{d})$, and $u_2|_{\mathcal{T}_e}$ is a first eigenfunction of $(\mathcal{T}_e, \mathbf{nn}\mathfrak{d})$.

(ii) For the eigenspace $\mathcal{E}(\nu_3)$ we have

$$(2.13) \quad \begin{cases} \dim(\mathcal{E}(\nu_3) \cap \mathcal{S}_{+,+}) = \dim(\mathcal{E}(\nu_3) \cap \mathcal{S}_{-,+}) = 1, \\ \mathcal{E}(\nu_3) \cap \mathcal{S}_{-,-} = \mathcal{E}(\nu_3) \cap \mathcal{S}_{+,-} = \{0\}. \end{cases}$$

In particular, the eigenspace $\mathcal{E}(\nu_3)$ is spanned by two linearly independent functions u_3 and u_4 which are M invariant, and whose restrictions to \mathcal{T}_e generate the eigenspace $\mathcal{E}(\nu_2(\mathcal{T}_e))$.

Proof. According to the Reflection principle, Proposition 2.1, the first six eigenvalues of $(\mathcal{R}h_e, \mathbf{n})$ belong to the set

$$(2.14) \quad \{\mu_i(\mathcal{T}_h, \mathbf{nab}) \text{ for } 1 \leq i \leq 6 \text{ and } \mathbf{a}, \mathbf{b} \in \{\mathfrak{d}, \mathbf{n}\}\}.$$

Among these numbers, the eigenvalues of $(\mathcal{T}_h, \mathbf{nnn})$ and $(\mathcal{T}_h, \mathbf{n}\mathfrak{d}\mathbf{n})$ are known explicitly, and they are simple, see Table 2.2.

Although the eigenvalues and eigenfunctions of $(\mathcal{T}_h, \mathbf{nn}\mathfrak{d})$ and $(\mathcal{T}_h, \mathfrak{d}\mathbf{n}\mathbf{n})$ are, as far as we know, not explicitly known, they satisfy some inequalities: the obvious inequalities $\mu_1 < \mu_2 \leq \dots$, and the inequalities provided by Proposition 2.2 (see [22]), and Proposition 2.3 (see [25]).

Table 2.4 summarizes what we know about the four first eigenvalues of the problems $(\mathcal{T}_h, \mathbf{nab})$, for $\mathbf{a}, \mathbf{b} \in \{\mathfrak{d}, \mathbf{n}\}$.

In blue the known values, in red the known inequalities (Propositions 2.2 and 2.3). The gray cells contain the eigenvalues, listed with multiplicities, for which we have no a priori information, except the trivial inequalities (black inequality signs).

Remark 2.8. Note that we only display the first four eigenvalues in each line, because this turns out to be sufficient for our purposes.

Remark 2.9. The reason why there are white empty cells in the 5th row is explained in Remark 2.4.

- We know that $\nu_1 = 0$, and that this eigenvalue is simple.
- From Table 2.4, we deduce that

$$\nu_2 \in \{\mu_2(\mathcal{T}_h, \mathbf{nnn}), \mu_1(\mathcal{T}_h, \mathbf{nn}\mathfrak{d})\},$$

with no other possibility. On the other hand, $\mu_1(\mathcal{T}_h, \mathbf{nn}\mathfrak{d}) < \mu_1(\mathcal{T}_h, \mathbf{n}\mathfrak{d}\mathbf{n}) = \mu_2(\mathcal{T}_h, \mathbf{nnn})$. It follows that $\nu_2 = \mu_1(\mathcal{T}_h, \mathbf{nn}\mathfrak{d})$, and that this eigenvalue is simple, $\nu_2 < \nu_3$.

TABLE 2.4. $\mathcal{R}h_e$, Neumann boundary condition

(σ, τ)	$(\mathcal{T}_h, \mathbf{na}\mathbf{b})$	μ_1		μ_2		μ_3		μ_4
$(+, +)$	$(\mathcal{T}_h, \mathbf{nnn})$	0	<	$\frac{16\pi^2}{9}$	<	$3 \frac{16\pi^2}{9}$	<	$4 \frac{16\pi^2}{9}$
Prop. 2.2		\wedge		\wedge		\wedge		\wedge
$(+, -)$	$(\mathcal{T}_h, \mathbf{nn}\mathbf{d})$		<		\leq		\leq	
Prop. 2.3		\wedge						
$(-, +)$	$(\mathcal{T}_h, \mathbf{n}\mathbf{d}\mathbf{n})$	$\frac{16\pi^2}{9}$	<	$4 \frac{16\pi^2}{9}$	<	$7 \frac{16\pi^2}{9}$	<	$9 \frac{16\pi^2}{9}$
Prop. 2.2		\wedge		\wedge		\wedge		\wedge
$(-, -)$	$(\mathcal{T}_h, \mathbf{n}\mathbf{d}\mathbf{d})$		<		\leq		\leq	

- From Table 2.4 and the knowledge of ν_1 and ν_2 , we deduce that

$$\nu_3 \in \{\mu_2(\mathcal{T}_h, \mathbf{nnn}), \mu_1(\mathcal{T}_h, \mathbf{n}\mathbf{d}\mathbf{n})\},$$

with no other possibility. Since $\mu_2(\mathcal{T}_h, \mathbf{nnn}) = \mu_1(\mathcal{T}_h, \mathbf{n}\mathbf{d}\mathbf{n})$, we have $\nu_3 = \nu_4 < \nu_5$. The proposition follows. \square

Note: For the reader's information, Table 2.5, displays numerical values for the eigenvalues: in the gray cells, the numerical values computed with MATLAB; in the other cells, the approximate values of the known eigenvalues.

TABLE 2.5. $\mathcal{R}h_e$, Neumann boundary condition

(σ, τ)	$(\mathcal{T}_h, \mathbf{na}\mathbf{b})$	μ_1		μ_2		μ_3		μ_4
$(+, +)$	$(\mathcal{T}_h, \mathbf{nnn})$	0	<	17.55	<	52.64	<	70.18
		\wedge		\wedge		\wedge		\wedge
$(+, -)$	$(\mathcal{T}_h, \mathbf{nn}\mathbf{d})$	7.16	<	37.49	\leq	90.06	\leq	120.87
		\wedge						
$(-, +)$	$(\mathcal{T}_h, \mathbf{n}\mathbf{d}\mathbf{n})$	17.55	<	70.18	<	122.82	<	157.91
		\wedge		\wedge		\wedge		\wedge
$(-, -)$	$(\mathcal{T}_h, \mathbf{n}\mathbf{d}\mathbf{d})$	47.63	<	110.36	\leq	189.52	\leq	224.68

Remark 2.10. One can also deduce Proposition 2.7 from the proof of Corollary 1.3 in [25] which establishes that the first four Neumann eigenvalues of a rhombus $\mathcal{R}h(\alpha)$ with smallest angle $2\alpha > \frac{\pi}{3}$ are simple, and describes the nodal patterns of the corresponding eigenvalues. When $2\alpha = \frac{\pi}{3}$ the eigenvalues ν_3 and ν_4 become equal, see also Remarks 4.1 and 4.2 in [25].

2.5. $\mathbf{ECP}(\mathcal{R}h_e, \mathbf{n})$ is false. As a corollary of Proposition 2.7, we obtain,

Proposition 2.11. *The Extended Courant property is false for the equilateral rhombus with Neumann boundary condition. More precisely, there exists a linear combination of eigenfunctions in $\mathcal{E}(\nu_1) \oplus \mathcal{E}(\nu_3)$ with four nodal domains.*

Proof. Proposition 2.7, Assertion (ii) tells us that $\mathcal{E}(\nu_3)$ contains an eigenfunction which arises from a second D -invariant Neumann eigenfunction of $\mathcal{T}_{e,1} = \mathcal{T}_e$. It suffices to apply the arguments of [9, Section 3.1], where we prove that $\text{ECP}(\mathcal{T}_0, \mathbf{n})$ is false. Here, \mathcal{T}_0 is the equilateral triangle with vertices $(0, 0)$, $(1, 0)$ and $(\frac{1}{2}, \frac{\sqrt{3}}{2})$. A second D -invariant Neumann eigenfunction for \mathcal{T}_0 is given by

$$(2.15) \quad \phi(x, y) = 2 \cos\left(\frac{2\pi x}{3}\right) \left(\cos\left(\frac{2\pi x}{3}\right) + \cos\left(\frac{2\pi y}{\sqrt{3}}\right) \right) - 1.$$

The linear combination $\phi + 1$ vanishes on the line segments $\{x = \frac{3}{4}\} \cap \mathcal{T}_0$ and $\{x + \sqrt{3}y = \frac{3}{2}\} \cap \mathcal{T}_0$.

Transplant the function ϕ to $\mathcal{T}_{e,1}$ by rotation and, using the symmetry with respect to M , extend it to an M -invariant eigenfunction u_3 for $(\mathcal{R}h_e, \mathbf{n})$. The linear combination $u_3 + 1$ vanishes on two line segments which divide $\mathcal{R}h_e$ into four nodal domains, see Figure 2.4. The proposition is proved. \square

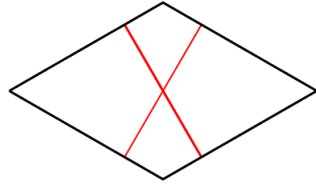


FIGURE 2.4. Nodal pattern of $u_3 + 1$, four nodal domains

Figure 2.5 illustrates the variation of the number of nodal domains (the eigenfunction produced by MATLAB is proportional to u_3 , not equal, so that the bifurcation value is not 1 as in the proof of Proposition 2.11).

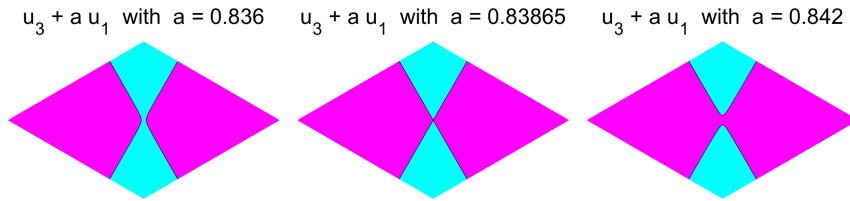


FIGURE 2.5. $(\mathcal{R}h_e, \mathbf{n})$: ECP false in $\mathcal{E}(\nu_1) \oplus \mathcal{E}(\nu_3)$

2.6. Numerical results for the $\text{ECP}(\mathcal{R}h_e, \mathbf{n})$. In Subsection 2.4, we have identified the first four eigenvalues of $(\mathcal{R}h_e, \mathbf{n})$, in particular $\nu_2 = \mu_1(\mathcal{T}_h, \mathbf{nnd})$. The numerical computations in Table 2.5 indicate that the next eigenvalues are $\nu_5 = \mu_2(\mathcal{T}_h, \mathbf{nnd}) = \mu_1(\mathcal{T}_h, \mathbf{nndd}) = \nu_6$, so that the Neumann eigenvalues of the equilateral rhombus satisfy,

$$(2.16) \quad 0 = \nu_1 < \nu_2 < \nu_3 = \nu_4 < \nu_5 < \nu_6 < \dots,$$

with corresponding nodal patterns shown in Figure 2.6. Looking at linear combinations of the form $u_5 + au_2$, see Figure 2.7, we obtain the following numerical result.

Statement 2.12. *Numerical computations of the eigenvalues and of the eigenfunctions indicate that the $\text{ECP}(\mathcal{R}h_e, \mathbf{n})$ is false in $\mathcal{E}(\nu_2) \oplus \mathcal{E}(\nu_5)$. More precisely, there exist linear combinations with six nodal domains.*

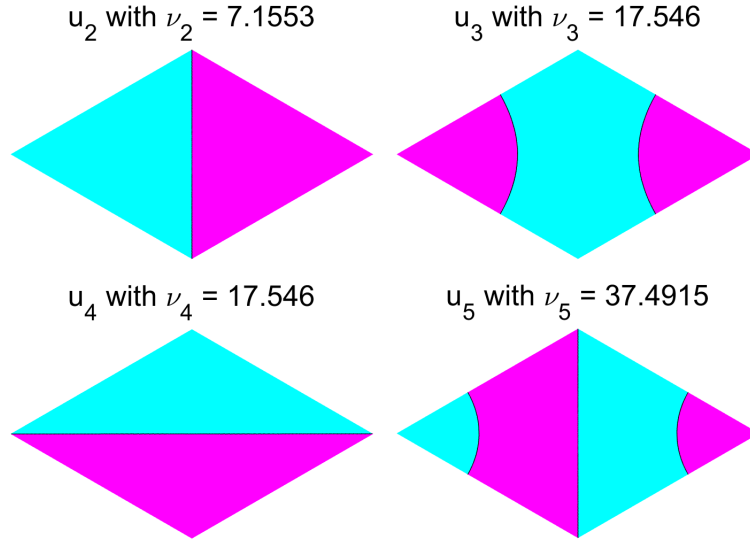


FIGURE 2.6. $(\mathcal{R}h_e, \mathbf{n})$: nodal patterns $u_2 - u_5$

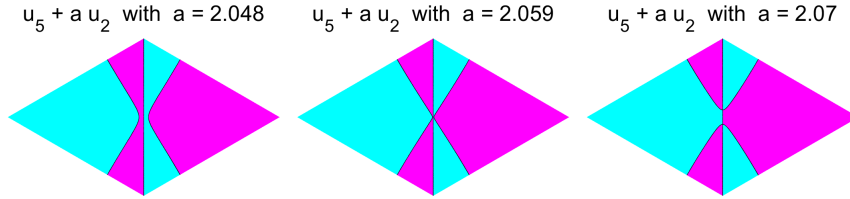
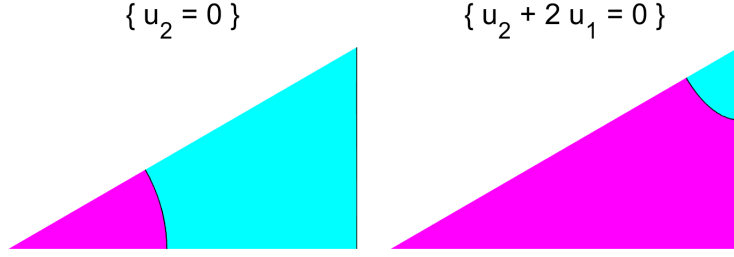


FIGURE 2.7. $(\mathcal{R}h_e, \mathbf{n})$: ECP false in $\mathcal{E}(\nu_2) \oplus \mathcal{E}(\nu_5)$

Remark 2.13. *This counterexample can also be interpreted as a counterexample to the ECP for the equilateral triangle with mixed boundary conditions, Neumann on two sides, and Dirichlet on the third side. We first look at nodal patterns in $\mathcal{E}(\mu_1(\mathcal{T}_h, \mathbf{nnd})) \oplus \mathcal{E}(\mu_2(\mathcal{T}_h, \mathbf{nnd}))$, see Figure 2.8. The corresponding nodal patterns in $\mathcal{E}(\mu_1(\mathcal{T}_e, \mathbf{nnd})) \oplus \mathcal{E}(\mu_2(\mathcal{T}_e, \mathbf{nnd}))$ are obtained using the symmetry with respect to the horizontal side.*

Remark 2.14. *We refer to Section 4 for comments on our numerical approach.*

FIGURE 2.8. $(\mathcal{T}_h, \mathbf{nn}\mathbf{d})$: nodal patterns in $\mathcal{E}(\mu_1) \oplus \mathcal{E}(\mu_2)$

2.7. Numerical results for the $\mathbf{ECP}(\mathcal{R}h_e, \mathbf{d})$. Table 2.6 is the analogue of Table 2.4 for the Dirichlet problem in $\mathcal{R}h_e$. Although one can identify the first two Dirichlet eigenvalues of $\mathcal{R}h_e$ as $\delta_1(\mathcal{R}h_e) = \mu_1(\mathcal{T}_h, \mathbf{dnn})$ and $\delta_2(\mathcal{R}h_e) = \mu_1(\mathcal{T}_h, \mathbf{dnd})$, it is not possible to rigorously identify the following eigenvalues. We have to rely on numerical computations.

TABLE 2.6. $\mathcal{R}h_e$, Dirichlet boundary condition

(σ, τ)	$(\mathcal{T}_h, \mathbf{dab})$	μ_1		μ_2		μ_3		μ_4
$(+, +)$	$(\mathcal{T}_h, \mathbf{dnn})$		$<$		\leq		\leq	
Prop. 2.2		\wedge		\wedge		\wedge		\wedge
$(+, -)$	$(\mathcal{T}_h, \mathbf{dnd})$	$3 \frac{16\pi^2}{9}$	$<$	$7 \frac{16\pi^2}{9}$	$<$	$12 \frac{16\pi^2}{9}$	$<$	$13 \frac{16\pi^2}{9}$
Prop. 2.3		\wedge						
$(-, +)$	$(\mathcal{T}_h, \mathbf{ddn})$		$<$		\leq		\leq	
Prop. 2.2		\wedge		\wedge		\wedge		\wedge
$(-, -)$	$(\mathcal{T}_h, \mathbf{ddd})$	$7 \frac{16\pi^2}{9}$	$<$	$13 \frac{16\pi^2}{9}$	$<$	$19 \frac{16\pi^2}{9}$	$<$	$21 \frac{16\pi^2}{9}$

Table 2.7 provides the numerical eigenvalues computed with MATLAB, and numerical approximations of the explicitly known eigenvalues.

TABLE 2.7. $\mathcal{R}h_e$, Dirichlet boundary condition

(σ, τ)	$(\mathcal{T}_h, \mathbf{dab})$	μ_1		μ_2		μ_3		μ_4
$(+, +)$	$(\mathcal{T}_h, \mathbf{dnn})$	24.90	$<$	83.83	\leq	140.50	\leq	169.20
		\wedge		\wedge		\wedge		\wedge
$(+, -)$	$(\mathcal{T}_h, \mathbf{dnd})$	52.64	$<$	122.82	$<$	210.55	$<$	228.10
		\wedge						
$(-, +)$	$(\mathcal{T}_h, \mathbf{ddn})$	71.71	$<$	169.80	\leq	234.10	\leq	292.70
		\wedge		\wedge		\wedge		\wedge
$(-, -)$	$(\mathcal{T}_h, \mathbf{ddd})$	122.82	$<$	228.10	$<$	333.37	$<$	368.47

From Table 2.7, we deduce that the Dirichlet eigenvalues of $\mathcal{R}h_e$ satisfy

$$(2.17) \quad 0 < \delta_1 < \delta_2 < \delta_3 < \delta_4 < \delta_5 = \delta_6 < \delta_7 \dots$$

More precisely, we find that $\delta_2(\mathcal{R}h_e) = \mu_1(\mathcal{T}_h, \mathbf{dnd}) = \delta_1(\mathcal{T}_e)$ (the first Dirichlet eigenvalue of the equilateral triangle \mathcal{T}_e). An eigenfunction u_2

associated with $\delta_2(\mathcal{R}h_e)$ arises from a first Dirichlet eigenfunction of \mathcal{T}_e . We also find that $\delta_5(\mathcal{R}h_e) = \mu_2(\mathcal{T}_h, \mathfrak{d}\mathfrak{n}\mathfrak{d}) = \mu_1(\mathcal{T}_h, \mathfrak{d}\mathfrak{d}\mathfrak{d}) = \delta_2(\mathcal{T}_e)$. Eigenfunctions associated with $\delta_5(\mathcal{R}h_e)$ arise from second Dirichlet eigenfunctions of \mathcal{T}_e , one of them u_5 is invariant with respect to D , the other is anti-invariant. The nodal patterns of u_2 and u_5 are given in Figure 2.9 (first and last pictures).

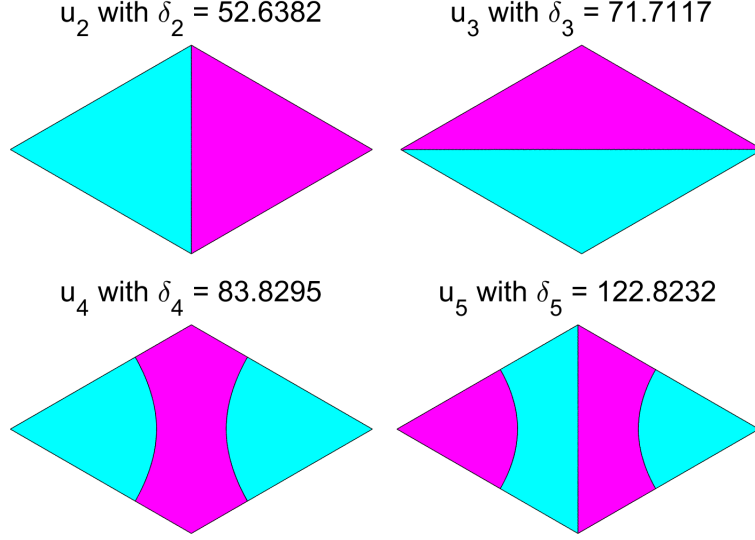


FIGURE 2.9. $(\mathcal{R}h_e, \mathfrak{d})$: nodal patterns $u_2 - u_5$

In [9, Section 3], we proved that $\text{ECP}(\mathcal{T}_e, \mathfrak{d})$ is false: there exists a linear combination of a first eigenfunction and a second D -invariant eigenfunction of $(\mathcal{T}_e, \mathfrak{d})$, with three nodal domains. The same example transcribed to $(\mathcal{R}h_e, \mathfrak{d})$ yields a linear combination in $\mathcal{E}(\delta_2) \oplus \mathcal{E}(\delta_5)$ with 6 nodal domains: for the Dirichlet problem in $\mathcal{R}h_e$, we have the following (numerical) analogue of Proposition 2.11, see Figure 2.10.

Statement 2.15. *The numerical approximations of the eigenvalues $\delta_j(\mathcal{R}h_e)$ deduced from Table 2.7 indicate that the $\text{ECP}(\mathcal{R}h_e, \mathfrak{d})$ is false in $\mathcal{E}(\delta_2) \oplus \mathcal{E}(\delta_5)$.*

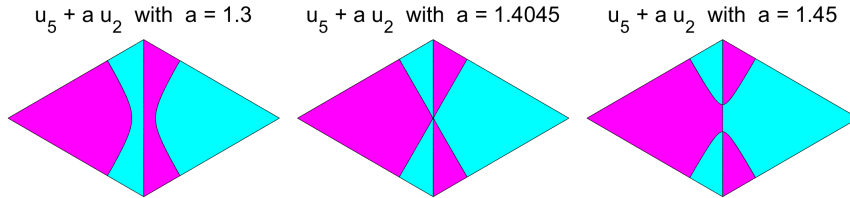


FIGURE 2.10. $(\mathcal{R}h_e, \mathfrak{d})$: ECP false in $\mathcal{E}(\delta_2) \oplus \mathcal{E}(\delta_5)$

Remark. We refer to Section 4 for comments on our numerical approach.

3. THE REGULAR HEXAGON

3.1. Symmetries and spectra. Let \mathcal{H} denote the interior of the regular hexagon with center at the origin, and sides of unit length. The diagonals $D_i, i = 1, 2, 3$, joining opposite vertices, and the medians $M_j, j = 1, 2, 3$, joining the mid-points of opposite sides, are lines of mirror symmetry of the hexagon \mathcal{H} , see Figure 3.1.

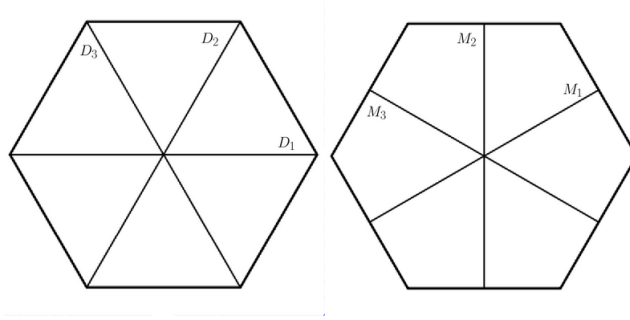


FIGURE 3.1. The hexagon and its mirror symmetries

We consider the diagonals D_1 and M_2 , and the associated mirror symmetries of \mathcal{H} . They commute,

$$(3.1) \quad M_2 \circ D_1 = D_1 \circ M_2 = R_\pi,$$

and we can therefore apply the methods of Subsection 2.1.

It follows that D_1^* leaves the subspaces $\mathcal{S}_{M_2, \pm}$ globally invariant, and that M_2^* leaves the subspaces $\mathcal{S}_{D_1, \pm}$ globally invariant. As a consequence, we have the following orthogonal decomposition of $L^2(\mathcal{H})$,

$$(3.2) \quad L^2(\mathcal{H}) = \mathcal{S}_{+,+} \oplus \mathcal{S}_{-,-} \oplus \mathcal{S}_{+,-} \oplus \mathcal{S}_{-,+},$$

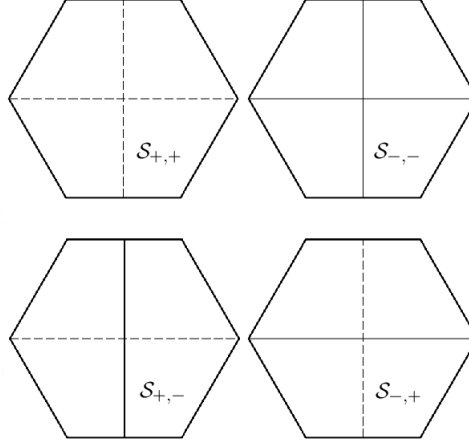
where

$$(3.3) \quad \mathcal{S}_{\sigma,\tau} := \left\{ \phi \in L^2(\mathcal{H}) \mid D_1^* \phi = \sigma \phi \text{ and } M_2^* \phi = \tau \phi \right\},$$

for $\sigma, \tau \in \{+, -\}$.

Similar decompositions hold for the Sobolev spaces $H^1(\mathcal{H})$ and $H_0^1(\mathcal{H})$, which are used in the variational presentation of the Neumann (resp. Dirichlet) eigenvalue problem for the hexagon. Since the Laplacian commutes with the isometries D_1 and M_2 , such decompositions also hold for the eigenspaces of $-\Delta$ in \mathcal{H} , with the boundary condition $\mathbf{b} \in \{\mathfrak{d}, \mathfrak{n}\}$ on the boundary $\partial\mathcal{H}$.

In the following figures, anti-nodal lines are indicated by dashed lines, and nodal lines by solid lines. Figure 3.2 displays the nodal and anti-nodal lines common to all functions in $H^1(\mathcal{H}) \cap \mathcal{S}_{\sigma,\tau}$, where $\sigma, \tau \in \{+, -\}$.

FIGURE 3.2. Spaces $\mathcal{S}_{\sigma,\tau}$ for $\sigma, \tau \in \{+, -\}$

Denote by R the rotation $R_{\frac{2\pi}{3}}$,

$$(3.4) \quad \begin{cases} R &= D_2 \circ D_1 = M_2 \circ M_1 = \dots, \\ R^{-1} &= D_1 \circ D_2 = M_1 \circ M_2 = \dots. \end{cases}$$

This is an isometry of \mathcal{H} , and the action R^* of R on functions is an isometry of $L^2(\mathcal{H})$ with respect to the L^2 -inner-product.

Lemma 3.1. *Let*

$$(3.5) \quad \begin{cases} \mathcal{S}^0 &:= \ker(R^* - I), \text{ and} \\ \mathcal{S}^1 &:= \ker(R^{*2} + R^* + I), \end{cases}$$

as subspaces of $L^2(\mathcal{H})$. Then

$$(3.6) \quad \begin{cases} \mathcal{S}^0 &= \text{img}(R^{*2} + R^* + I) = \ker(R^{*2} + R^* + I)^\perp, \\ \mathcal{S}^1 &= \text{img}(R^* - I) = \ker(R^* - I)^\perp, \end{cases}$$

and we have the orthogonal decomposition

$$(3.7) \quad L^2(\mathcal{H}) = \mathcal{S}^0 \overset{\perp}{\oplus} \mathcal{S}^1.$$

Here, as usual, $\text{img}(f)$ and $\ker(f)$ denote respectively the image and the kernel of the linear map f , and E^\perp the subspace orthogonal to E .

Proof. The following polynomial identities hold.

$$(3.8) \quad x^3 - 1 = (x - 1)(x^2 + x + 1),$$

$$(3.9) \quad 3 = (x^2 + x + 1) - (x - 1)(x + 2).$$

Furthermore, the rotation R satisfies

$$(3.10) \quad R^3 = I.$$

From (3.8) and (3.10), we deduce that

$$(3.11) \quad \text{img}(R^{*2} + R^* + I) \subset \ker(R^* - I),$$

and

$$(3.12) \quad \text{img}(R^* - I) \subset \ker(R^{*2} + R + I).$$

From (3.9), we deduce that

$$(3.13) \quad L^2(\mathcal{H}) = \text{img}(R^* - I) + \text{img}(R^{*2} + R + I),$$

and hence, using (3.11) and (3.12)

$$(3.14) \quad L^2(\mathcal{H}) = \ker(R^* - I) + \ker(R^{*2} + R + I).$$

Clearly,

$$(3.15) \quad \ker(R^* - I) \cap \ker(R^{*2} + R + I) = \{0\},$$

so that, using (3.11) and (3.12),

$$(3.16) \quad \text{img}(R^* - I) \cap \text{img}(R^{*2} + R + I) = \{0\}.$$

Let $\phi \in \text{img}(R^* - I)$ and $\psi \in \text{img}(R^{*2} + R + I)$. Using the fact that R^* is an isometry and (3.10), we conclude that $\langle \phi, \psi \rangle = 0$ (the L^2 inner product). Therefore,

$$(3.17) \quad \text{img}(R^* - I) = \text{img}(R^{*2} + R + I)^\perp.$$

From the previous identities, we deduce that

$$(3.18) \quad L^2(\mathcal{H}) = \text{img}(R^* - I) \overset{\perp}{\oplus} \text{img}(R^{*2} + R + I),$$

$$(3.19) \quad L^2(\mathcal{H}) = \ker(R^* - I) \overset{\perp}{\oplus} \ker(R^{*2} + R + I),$$

$$(3.20) \quad \text{img}(R^* - I) = \ker(R^{*2} + R + I),$$

$$(3.21) \quad \text{img}(R^{*2} + R + I) = \ker(R^* - I).$$

The lemma is proved. \square

Lemma 3.2. For $\sigma, \tau \in \{+, -\}$, using the notation (3.5), define the subspaces

$$(3.22) \quad \begin{cases} \mathcal{S}_{\sigma, \tau}^0 &:= \mathcal{S}_{\sigma, \tau} \cap \mathcal{S}^0, \\ \mathcal{S}_{\sigma, \tau}^1 &:= \mathcal{S}_{\sigma, \tau} \cap \mathcal{S}^1. \end{cases}$$

Define the map

$$(3.23) \quad \begin{cases} T : L^2(\mathcal{H}) \rightarrow L^2(\mathcal{H}), \\ T(\phi) = R^* \phi - R^{*2} \phi. \end{cases}$$

Then,

- (1) $\ker(T) = \mathcal{S}^0$ and $\ker(T)^\perp = \mathcal{S}^1$.
- (2) $T^2 = (R^{*2} + R^* + I) - 3I$; $T \circ T|_{\mathcal{S}^1} = -3I$; $T(\mathcal{S}^1) = \mathcal{S}^1$; T is a bijection from \mathcal{S}^1 onto \mathcal{S}^1 .

(3) $T \circ \Delta = \Delta \circ T$, so that T leaves the eigenspaces of Δ globally invariant.

(4) For all $\sigma, \tau \in \{+, -\}$, the subspace $\mathcal{S}_{\sigma, \tau}^0$ satisfies

$$(3.24) \quad \mathcal{S}_{\sigma, \tau}^0 = \left\{ \phi \in L^2(\mathcal{H}) \mid D_i^* \phi = \sigma \phi, M_j^* \phi = \tau \phi, 1 \leq i, j \leq 3 \right\}.$$

(5) For all $\sigma, \tau \in \{+, -\}$, $T(\mathcal{S}_{\sigma, \tau}) \subset \mathcal{S}_{-\sigma, -\tau}$.

(6) For all $\sigma, \tau \in \{+, -\}$, $\ker(T|_{\mathcal{S}_{\sigma, \tau}}) = \mathcal{S}_{\sigma, \tau}^0$, and $\text{img}(T|_{\mathcal{S}_{\sigma, \tau}}) \subset \mathcal{S}_{-\sigma, -\tau}^1$.

(7) For all $\sigma, \tau \in \{+, -\}$,

$$(3.25) \quad \mathcal{S}_{\sigma, \tau} = \mathcal{S}_{\sigma, \tau}^0 \overset{\perp}{\oplus} \mathcal{S}_{\sigma, \tau}^1,$$

and T is a bijection from $\mathcal{S}_{\sigma, \tau}^1$ onto $\mathcal{S}_{-\sigma, -\tau}^1$.

Proof. Assertion (1) If $\phi \in \ker(T)$, then $R^{*2}\phi = R^*\phi$, so that $\phi = R^{*3}\phi = R^{*2}\phi = R^*\phi$, and $\phi \in \mathcal{S}^0$. The converse is clear. The second equality follows from Lemma 3.1.

Assertion (2) The first two equalities are clear. If $\phi \in \mathcal{S}^1$, then $(R^{*2} + R^* + I)T(\phi) = (R^{*2} + R^* + I)(R^* - I)R^*\phi = 0$, and $T(\phi) \in \mathcal{S}^1$. If $\phi \in \mathcal{S}^1$, then $T(T(\phi)) = -3\phi$, so that $\phi = T(\psi)$ with $\psi = -\frac{1}{3}T(\phi) \in \mathcal{S}^1$. This implies that $T(\mathcal{S}^1) = \mathcal{S}^1$. On the other hand, if $T(\phi) = 0$ and $\phi \in \mathcal{S}^1$, then $\phi \in \mathcal{S}^0 \cap \mathcal{S}^1 = \{0\}$.

Assertion (3) This assertion is clear because R is an isometry, so that R^* commutes with Δ . It follows that T commutes with Δ as well, and hence that T leaves each eigenspace $\mathcal{E}(\lambda)$ globally invariant.

Assertion (4) Let $\phi \in \mathcal{S}_{\sigma, \tau}^0$. Then $R^*\phi = \phi$ and $D_1^*\phi = \sigma\phi$. Since $R = D_1 \circ D_3$, it follows that $\phi = R^*\phi = D_3^*D_1^*\phi = \sigma D_3^*\phi$, so that $D_3^*\phi = \sigma\phi$. The other equalities are established in a similar way. On the other hand, if $D_1^*\phi = D_3^*\phi = \sigma\phi$, then

$$R^*\phi = (D_1 \circ D_3)^*\phi = \sigma^2\phi = \phi.$$

Assertion (5) Let $\phi \in \mathcal{S}_{\sigma, \tau}$, i.e., $D_1^*\phi = \sigma\phi$ and $M_2^*\phi = \tau\phi$. Then,

$$\begin{aligned} D_1^*(T(\phi)) &= D_1^*R^*\phi - D_1^*R^{*2}\phi \\ &= D_1^*(D_2 \circ D_1)^*\phi - D_1^*(D_3 \circ D_1)^*\phi \\ &= D_2^*\phi - D_3^*\phi \\ &= (D_1 \circ D_1 \circ D_2)^*\phi - (D_1 \circ D_1 \circ D_3)^*\phi \\ &= (D_1 \circ D_2)^*D_1^*\phi - (D_1 \circ D_3)^*D_1^*\phi \\ &= \sigma R^{*2}\phi - \sigma R^*\phi \\ &= -\sigma T(\phi). \end{aligned}$$

Similarly, one shows that $M_2^*(T(\phi)) = -\tau T(\phi)$.

Assertion (6) The first equality follows from Assertion (1). The second equality follows from Assertion (5) and the fact that $\text{img}(T) \subset \mathcal{S}^1$ because $R^{*3} = I$.

Assertion (γ) Take $\phi \in \mathcal{S}_{\sigma,\tau}$. Then $T(\phi) \in \mathcal{S}^1 \cap \mathcal{S}_{-\sigma,-\tau}$ and hence $T^2(\phi) \in \mathcal{S}^1 \cap \mathcal{S}_{\sigma,\tau}$. We also have $T^2(\phi) = (R^{*2} + R^* + I)(\phi) - 3\phi$, which implies that $(R^{*2} + R^* + I)(\phi) \in \mathcal{S}^0 \cap \mathcal{S}_{\sigma,\tau}$. The initial equality can be rewritten $\phi = \frac{1}{3}(R^{*2} + R^* + I)(\phi) - \frac{1}{3}T^2(\phi)$ which implies that $\mathcal{S}_{\sigma,\tau} = \mathcal{S}^0 \cap \mathcal{S}_{\sigma,\tau} \oplus \mathcal{S}^1 \cap \mathcal{S}_{\sigma,\tau}$.

We have $T(\mathcal{S}^1 \cap \mathcal{S}_{\sigma,\tau}) \subset \mathcal{S}^1 \cap \mathcal{S}_{-\sigma,-\tau}$. If $\phi \in \mathcal{S}^1 \cap \mathcal{S}_{\sigma,\tau}$ and $T(\phi) = 0$, then $\phi \in \mathcal{S}^0 \cap \mathcal{S}^1 = \{0\}$. If $\phi \in \mathcal{S}^1 \cap \mathcal{S}_{-\sigma,-\tau}$, then $\phi = T(\psi)$ with $\psi = -\frac{1}{3}T(\phi) \in \mathcal{S}^1 \cap \mathcal{S}_{\sigma,\tau}$. This proves that T is bijective. \square

Figure 3.3 displays the nodal and anti-nodal lines common to all functions in $H^1(\mathcal{H}) \cap \mathcal{S}_{\sigma,\tau}^0$, with $\sigma, \tau \in \{+, -\}$.

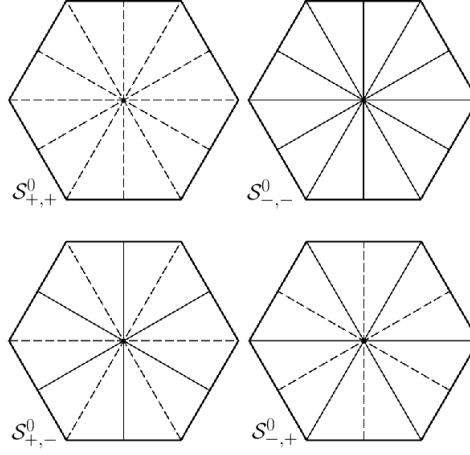


FIGURE 3.3. The spaces $\mathcal{S}_{\sigma,\tau}^0$ for $\sigma, \tau \in \{+, -\}$

The Laplacian Δ commutes with isometries. It follows that the eigenspaces of the Laplacian Δ in \mathcal{H} , with either the Neumann or Dirichlet boundary condition on $\partial\mathcal{H}$, decompose orthogonally according to the spaces $\mathcal{S}_{\sigma,\tau}$, \mathcal{S}^0 and \mathcal{S}^1 . More precisely, if $\mathcal{E}(\lambda)$ is the eigenspace of $-\Delta$ for the eigenvalue λ in the Neumann (resp. Dirichlet) spectrum of Δ , then

$$(3.26) \quad \mathcal{E}(\lambda) = \bigoplus_{\sigma,\tau \in \{+,-\}}^{\perp} \left(\mathcal{E}(\lambda) \cap \mathcal{S}_{\sigma,\tau}^0 \right) \bigoplus^{\perp} \left(\mathcal{E}(\lambda) \cap \mathcal{S}_{\sigma,\tau}^1 \right).$$

Remark 3.3. If $\mathcal{E}(\lambda) \cap \mathcal{S}_{\sigma,\tau}^1$ has dimension p , then by Lemma 3.2, $\mathcal{E}(\lambda) \cap \mathcal{S}_{-\sigma,-\tau}^1$ has dimension p . It follows that $\mathcal{E}(\lambda)$ has dimension at least $2p$.

Remark 3.4. Let λ be a simple eigenvalue. Then, any associated eigenfunction ϕ is either invariant or anti-invariant under any mirror symmetry L which leaves \mathcal{H} invariant, and invariant under R^* . It follows that $\phi \in \mathcal{S}_{\sigma,\tau}^0$ for some pair (σ, τ) .

Remark 3.5. Assume that $\phi \in \mathcal{E}(\lambda) \cap \mathcal{S}_{\sigma,\tau}^0$. Then, by Courant's theorem, we have $6 \leq \beta_0(\phi) \leq \kappa(\lambda)$ if $(\sigma, \tau) = (+, -)$ or $(-, +)$, and $12 \leq \beta_0(\phi) \leq \kappa(\lambda)$ if $(\sigma, \tau) = (-, -)$. If $\phi \in \mathcal{S}_{+,+}^0$, then ϕ arises from an eigenfunction of \mathcal{T}_h with Neumann boundary condition on the sides 1 and 2.

3.2. Symmetries and boundary conditions on sub-domains. Let \mathcal{Q} (resp. \mathcal{P}) denote the interior of the quadrilateral (resp. the pentagon) which appears in Figure 3.4. Let \mathcal{R} (resp. \mathcal{T}_h) denote the interior of the quadrilateral (resp. of the hemiequilateral triangle) which appears in Figure 3.5. Then, $\overline{\mathcal{Q}}$ (resp. $\overline{\mathcal{P}}$) is a fundamental domain of the action of the mirror symmetry D_1 (resp. M_2), and $\overline{\mathcal{R}}$ is a fundamental domain for the action of the group generated by D_1 and M_2 .

Using the notation of Subsection 2.1, we consider the following mixed eigenvalue problems in the domains $\mathcal{H}, \mathcal{P}, \mathcal{Q}$ and \mathcal{R} .

- For the hexagon \mathcal{H} , we do not decompose the boundary,

$$(3.27) \quad \partial\mathcal{H} = \Gamma_{\mathcal{H},1},$$

and we consider the eigenvalue problem $(\mathcal{H}, \mathbf{b})$ with $\mathbf{b} \in \{\mathbf{n}, \mathbf{d}\}$.

- For the quadrilateral \mathcal{Q} , we decompose the boundary as

$$(3.28) \quad \begin{cases} \partial\mathcal{Q} &= \overline{\Gamma_{\mathcal{Q},1} \sqcup \Gamma_{\mathcal{Q},2}}, \text{ with} \\ \Gamma_{\mathcal{Q},1} &= \overline{\mathcal{Q}} \cap D_1, \\ \Gamma_{\mathcal{Q},2} &= \overline{\mathcal{Q}} \cap \partial\mathcal{H}, \end{cases}$$

and we consider the eigenvalue problems $(\mathcal{Q}, \mathbf{ab})$, with $\mathbf{a}, \mathbf{b} \in \{\mathbf{n}, \mathbf{d}\}$.

- For the pentagon \mathcal{P} , we decompose the boundary as

$$(3.29) \quad \begin{cases} \partial\mathcal{P} &= \overline{\Gamma_{\mathcal{P},1} \sqcup \Gamma_{\mathcal{P},2}}, \text{ with} \\ \Gamma_{\mathcal{P},1} &= \overline{\mathcal{P}} \cap M_2, \\ \Gamma_{\mathcal{P},2} &= \overline{\mathcal{P}} \cap \partial\mathcal{H}, \end{cases}$$

and we consider the eigenvalue problems $(\mathcal{P}, \mathbf{ab})$, with $\mathbf{a}, \mathbf{b} \in \{\mathbf{n}, \mathbf{d}\}$.

- For the quadrilateral \mathcal{R} , we decompose the boundary as

$$(3.30) \quad \begin{cases} \partial\mathcal{R} &= \overline{\Gamma_{\mathcal{R},1} \sqcup \Gamma_{\mathcal{R},2} \sqcup \Gamma_{\mathcal{R},3}}, \text{ with} \\ \Gamma_{\mathcal{R},1} &= \overline{\mathcal{R}} \cap M_2, \\ \Gamma_{\mathcal{R},2} &= \overline{\mathcal{R}} \cap D_1, \\ \Gamma_{\mathcal{R},3} &= \overline{\mathcal{R}} \cap \partial\mathcal{H}, \end{cases}$$

and we consider the eigenvalue problems $(\mathcal{R}, \mathbf{abc})$, with $\mathbf{a}, \mathbf{b}, \mathbf{c} \in \{\mathbf{n}, \mathbf{d}\}$.

- We also consider the hemiequilateral triangle \mathcal{T}_h , its sides ordered in decreasing order of length, and the eigenvalue problems $(\mathcal{T}_h, \mathbf{abc})$, with $\mathbf{a}, \mathbf{b}, \mathbf{c} \in \{\mathbf{n}, \mathbf{d}\}$. For the equilateral triangle \mathcal{T}_e , up to isometry, it is not

necessary to order the sides, and we consider the eigenvalue problems $(\mathcal{T}_e, \mathbf{abc})$ with $\mathbf{a}, \mathbf{b}, \mathbf{c} \in \{\mathbf{n}, \mathbf{d}\}$.

The boundary decompositions for the domains $\mathcal{P}, \mathcal{Q}, \mathcal{R}$, and for the hemiequilateral triangle \mathcal{T}_h , are illustrated in Figures 3.4 and 3.5.

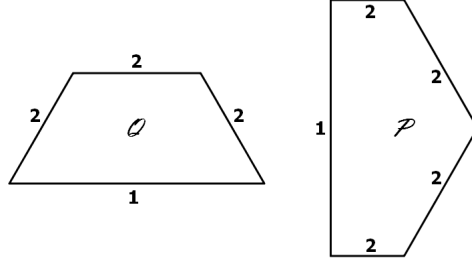


FIGURE 3.4. The sub-domains \mathcal{Q} and \mathcal{P}

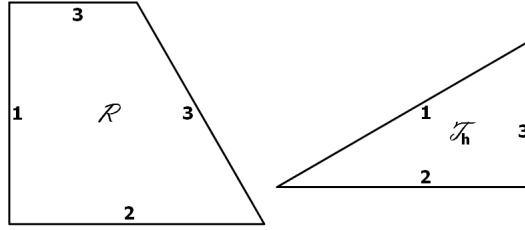


FIGURE 3.5. The sub-domains \mathcal{R} and \mathcal{T}_h

Consider the eigenvalue problem $(\mathcal{H}, \mathbf{c})$ for the hexagon, with $\mathbf{c} \in \{\mathbf{n}, \mathbf{d}\}$. Let $\mathcal{E}(\mu, \mathbf{c})$ be an eigenspace of $-\Delta$ for $(\mathcal{H}, \mathbf{c})$. If $\phi \in \mathcal{E}(\mu, \mathbf{c}) \cap \mathcal{S}_{\sigma, \tau}$, then the restriction $\phi|_{\mathcal{R}}$, of the function ϕ to the domain \mathcal{R} , is an eigenfunction of $-\Delta$ in $(\mathcal{R}, \varepsilon(\sigma)\varepsilon(\tau)\mathbf{c})$, where

$$(3.31) \quad \varepsilon(+)=\mathbf{n} \text { and } \varepsilon(-)=\mathbf{d},$$

associated with the same eigenvalue μ .

Conversely, let ψ be an eigenfunction of $-\Delta$ in $(\mathcal{R}, \mathbf{abc})$, associated with the eigenvalue μ , where \mathbf{c} is the given boundary condition on $\partial \mathcal{H}$, and $\mathbf{a}, \mathbf{b} \in \{\mathbf{d}, \mathbf{n}\}$ are boundary conditions on the sides M_2, D_1 . Extend ψ to a function $\check{\psi}$ defined on \mathcal{H} , by symmetry (resp. anti-symmetry) with respect to M_2 , if $\mathbf{a} = \mathbf{n}$ (resp. if $\mathbf{a} = \mathbf{d}$), and by symmetry (resp. anti-symmetry) with respect to D_1 , if $\mathbf{b} = \mathbf{n}$ (resp. if $\mathbf{b} = \mathbf{d}$). Then, the function $\check{\psi}$ is an eigenfunction of $-\Delta$ for $(\mathcal{H}, \mathbf{c})$, associated with the eigenvalue μ , and belongs to $\mathcal{S}_{\sigma, \tau}$ with $\varepsilon(\sigma) = \mathbf{a}$ and $\varepsilon(\tau) = \mathbf{b}$.

As in Subsection 2.1, we have,

Proposition 3.6. *The eigenvalues and eigenfunctions of $(\mathcal{H}, \mathfrak{c})$ in $\mathcal{S}_{\sigma, \tau}$ are in bijection with the eigenvalues and eigenfunctions of $(\mathcal{R}, \mathfrak{abc})$, with the boundary condition \mathfrak{a} on M_2 , with $\mathfrak{a} = \mathfrak{d}$, if $\sigma = -$, and $\mathfrak{a} = \mathfrak{n}$, if $\sigma = +$; and, similarly, with the boundary condition \mathfrak{b} on D_1 , with $\mathfrak{b} = \mathfrak{d}$, if $\tau = -$, and $\mathfrak{b} = \mathfrak{n}$, if $\tau = +$. Similar statements hold for \mathcal{P} , \mathcal{Q} and \mathcal{T}_h respectively.*

3.3. Identification of the first Dirichlet eigenvalues of the regular hexagon. Throughout this section, we fix the Dirichlet boundary condition \mathfrak{d} on $\partial\mathcal{H}$, and we denote the Dirichlet eigenvalues of \mathcal{H} by

$$(3.32) \quad \delta_1(\mathcal{H}) < \delta_2(\mathcal{H}) \leq \delta_3(\mathcal{H}) \leq \dots \leq \delta_6(\mathcal{H}) \leq \delta_7(\mathcal{H}) \leq \dots,$$

and the Dirichlet spectrum of the hexagon by $\text{sp}(\mathcal{H}, \mathfrak{d})$.

3.3.1. Numerical computations. Numerical approximations for the Dirichlet eigenvalues of the regular hexagon have been obtained by several authors, see for example [5, 16, 13], or the recent paper [17].

The main idea, in order to make the identification of multiple Dirichlet eigenvalues of \mathcal{H} easier, is to take the symmetries of \mathcal{H} (see Section 3.2) into account from the start. For this purpose, one computes the eigenvalues of the domains \mathcal{R} and \mathcal{T}_h , for mixed boundary conditions \mathfrak{abd} , with $\mathfrak{a}, \mathfrak{b} \in \{\mathfrak{d}, \mathfrak{n}\}$.

Table 3.1 displays the first four eigenvalues of $(\mathcal{R}, \mathfrak{abd})$, as computed with MATLAB, and contains some useful relations between these eigenvalues.

TABLE 3.1. \mathcal{R} -shape, mixed boundary conditions, first four approximate eigenvalues

$(\mathcal{R}, \mathfrak{abd})$	μ_1	$<$	μ_2	\leq	μ_3	\leq	μ_4
nn\mathfrak{d}	7.16	$<$	32.45	\leq	37.49	\leq	70.14
	\wedge		\wedge		\wedge		\wedge
d$\mathfrak{n}$$\mathfrak{d}$	18.13	$<$	47.63	\leq	60.11	\leq	94.33
	?		?		?		?
n$\mathfrak{d}$$\mathfrak{d}$	18.13	$<$	52.64	\leq	60.11	\leq	94.33
	\wedge		\wedge		\wedge		\wedge
d$\mathfrak{d}$$\mathfrak{d}$	32.45	$<$	70.14	\leq	87.53	\leq	122.82

Remark 3.7. *The eigenvalues in Table 3.1 are partially ordered ‘vertically’. Indeed, for $i \geq 1$, we have the strict inequalities,*

$$(3.33) \quad \begin{cases} \mu_i(\mathcal{R}, \mathfrak{nn}\mathfrak{d}) < \mu_i(\mathcal{R}, \mathfrak{d}\mathfrak{n}\mathfrak{d}) < \mu_i(\mathcal{R}, \mathfrak{d}\mathfrak{d}\mathfrak{d}), \\ \mu_i(\mathcal{R}, \mathfrak{nn}\mathfrak{d}) < \mu_i(\mathcal{R}, \mathfrak{n}\mathfrak{d}\mathfrak{d}) < \mu_i(\mathcal{R}, \mathfrak{d}\mathfrak{d}\mathfrak{d}), \end{cases}$$

which follow from Proposition 2.2, see [22, Proposition 2.3]. These inequalities are indicated in the table by the (rotated) strict inequality

signs. Note that it is in general not possible to compare the eigenvalues $\mu_i(\mathcal{R}, \mathfrak{d}\mathfrak{n}\mathfrak{d})$ and $\mu_i(\mathcal{R}, \mathfrak{n}\mathfrak{d}\mathfrak{d})$. This is indicated in the table by the black question marks.

Table 3.2 displays some eigenvalues of $(\mathcal{T}_h, \mathfrak{a}\mathfrak{b}\mathfrak{d})$, for $\mathfrak{a}, \mathfrak{b} \in \{\mathfrak{d}, \mathfrak{n}\}$. The lower bound in the second line follows from Dirichlet monotonicity (see Subsection 3.3.2). In the third line, we have used the fact due to Pólya (see [19]) that the first Dirichlet eigenvalue of a kite-shape is bounded from below by the first Dirichlet eigenvalue of a square with the same area. In the last two lines, the eigenvalues are known explicitly.

TABLE 3.2. Some eigenvalues of the hemiequilateral triangle

\mathcal{S}	$(\mathcal{T}_h, \mathfrak{a}\mathfrak{b}\mathfrak{d})$	Eigenvalue	Value
$\mathcal{S}_{+,+}^0$	$(\mathcal{T}_h, \mathfrak{n}\mathfrak{n}\mathfrak{d})$	μ_1	$\mu_1 \approx 7.16$
$\mathcal{S}_{+,+}^0$	$(\mathcal{T}_h, \mathfrak{n}\mathfrak{n}\mathfrak{d})$	μ_2	$\mu_2 \approx 37.49 > 26.37$
$\mathcal{S}_{+,-}^0$	$(\mathcal{T}_h, \mathfrak{n}\mathfrak{d}\mathfrak{d})$	μ_1	$\mu_1 \geq \frac{4\pi^2}{\sqrt{3}} \approx 22.79$
$\mathcal{S}_{-,+}^0$	$(\mathcal{T}_h, \mathfrak{d}\mathfrak{n}\mathfrak{d})$	μ_1	$\mu_1 = 3 \frac{16\pi^2}{9} \approx 52.64$
$\mathcal{S}_{-,-}^0$	$(\mathcal{T}_h, \mathfrak{d}\mathfrak{d}\mathfrak{d})$	μ_1	$\mu_1 = 7 \frac{16\pi^2}{3} \approx 122.82$

Remark 3.8. The figures in Table 3.1 suggest that the Dirichlet eigenvalues of \mathcal{H} come into four well separated sets $\{\delta_1(\mathcal{H})\}$, $\{\delta_2(\mathcal{H}), \delta_3(\mathcal{H})\}$, $\{\delta_4(\mathcal{H}), \delta_5(\mathcal{H})\}$ and $\{\delta_6(\mathcal{H})\}$.

3.3.2. *Lower and upper bounds for the Dirichlet eigenvalues.* The hexagon \mathcal{H} is inscribed in the unit disk \mathcal{D} , and contains the disk with radius $\frac{\sqrt{3}}{2}$. By domain monotonicity for the Dirichlet eigenvalues, we have the following lower and upper bounds for the Dirichlet eigenvalues of \mathcal{H} ,

$$(3.34) \quad \delta_j(\mathcal{D}) < \delta_j(\mathcal{H}) < \frac{4}{3} \delta_j(\mathcal{D}) \text{ for any } j \geq 1.$$

The Dirichlet eigenvalues of the unit disk \mathcal{D} satisfy the relations

$$(3.35) \quad \begin{cases} j_{0,1}^2 = \delta_1(\mathcal{D}) < j_{1,1}^2 = \delta_2(\mathcal{D}) = \delta_3(\mathcal{D}) \\ < j_{2,1}^2 = \delta_4(\mathcal{D}) = \delta_5(\mathcal{D}) < j_{0,2}^2 = \delta_6(\mathcal{D}) \\ < j_{3,1}^2 = \delta_7(\mathcal{D}) = \delta_8(\mathcal{D}) < \dots \end{cases}$$

where $j_{m,n}$ is the n -th positive zero of the Bessel function J_m .

Corresponding eigenfunctions are given by

$$(3.36) \quad \begin{cases} \delta_1(\mathcal{D}) \rightsquigarrow J_0(j_{0,1}r), \\ \delta_2(\mathcal{D}) \rightsquigarrow J_1(j_{1,1}r) \cos(\theta) \text{ and } J_1(j_{1,1}r) \sin(\theta), \\ \delta_4(\mathcal{D}) \rightsquigarrow J_2(j_{2,1}r) \cos(2\theta) \text{ and } J_2(j_{2,1}r) \sin(2\theta), \\ \delta_6(\mathcal{D}) \rightsquigarrow J_0(j_{0,2}r), \\ \delta_7(\mathcal{D}) \rightsquigarrow J_3(j_{3,1}r) \cos(3\theta) \text{ and } J_3(j_{3,1}r) \sin(3\theta). \end{cases}$$

with the nodal patterns represented in Figure 3.6.

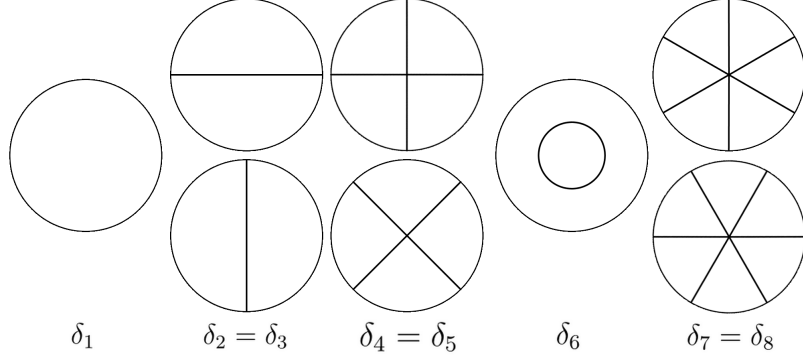


FIGURE 3.6. Nodal patterns in the first five Dirichlet eigenspaces of the unit disk

The lower and upper bounds (3.34) for the first eight eigenvalues are summarized in Table 3.3.

TABLE 3.3. Bounds for the first eight Dirichlet eigenvalues of the hexagon, using domain monotonicity

Eigenvalue	Lower bound	Upper bound
$\delta_1(\mathcal{H})$	5.78	7.72
$\delta_2(\mathcal{H}), \delta_3(\mathcal{H})$	14.68	19.58
$\delta_4(\mathcal{H}), \delta_5(\mathcal{H})$	26.37	35.17
$\delta_6(\mathcal{H})$	30.47	40.63
$\delta_7(\mathcal{H}), \delta_8(\mathcal{H})$	40.70	54.28

Similar bounds can be given for the first Dirichlet eigenvalues of the domains \mathcal{P} , \mathcal{Q} and \mathcal{R} , see Table 3.4.

TABLE 3.4. Bounds for the first Dirichlet eigenvalues of \mathcal{P} , \mathcal{Q} and \mathcal{R} , using domain monotonicity

Eigenvalue	Lower bound	Upper bound
$\delta_1(\mathcal{Q}), \delta_1(\mathcal{P})$	14.68	19.58
$\delta_1(\mathcal{R})$	26.37	35.17

It is easy to compute the eigenvalues of a sector of the unit disk, with Neumann boundary condition on the sides of the sector, and Dirichlet boundary condition on the arc of circle. In particular, the first (resp. second) eigenvalue of such a mixed Neumann-Dirichlet problem in the circular sector of angle $\frac{\pi}{6}$ is $j_{0,1}^2$ (resp. $j_{0,2}^2$). From domain monotonicity, we can compare the eigenvalues of $(\mathcal{T}_h, \mathbf{nnd})$ with the eigenvalues of the sectors with angle $\frac{\pi}{6}$, and respective radii $\frac{\sqrt{3}}{2}$ and 1, with the Neumann boundary condition on the boundary radii, and with the

Dirichlet boundary condition on the arc of circle, see Figure 3.7. We obtain the inequalities

$$(3.37) \quad \begin{cases} 5.78 < j_{0,1}^2 < \mu_1(\mathcal{T}_h, \mathbf{nn}\mathfrak{d}) \approx 7.16 < \frac{4}{3}j_{0,1}^2 < 7.72, \\ 30.47 < j_{0,2}^2 < \mu_2(\mathcal{T}_h, \mathbf{nn}\mathfrak{d}) \approx 37.49 < \frac{4}{3}j_{0,2}^2 < 40.63. \end{cases}$$

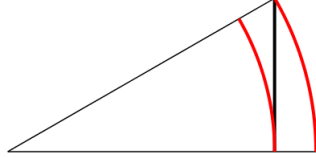


FIGURE 3.7. Domain monotonicity

Taking into account the bounds given in Table 3.3, we have the relations,

$$(3.38) \quad \begin{cases}]5.78, 7.72[\cap \sigma(\mathcal{H}, d) &= \{\delta_1(\mathcal{H})\}, \\]14.68, 19.58[\cap \sigma(\mathcal{H}, d) &= \{\delta_2(\mathcal{H}), \delta_3(\mathcal{H})\}, \\]26.37, 40.63[\cap \sigma(\mathcal{H}, d) &= \{\delta_4(\mathcal{H}), \delta_5(\mathcal{H}), \delta_6(\mathcal{H})\}, \\ 40.70 &\leq \delta_7(\mathcal{H}). \end{cases}$$

Subsection 3.2, the bounds provided by Table 3.4, and inequalities (3.37), imply that

$$(3.39) \quad \begin{cases} \mu_1(\mathcal{T}_h, \mathbf{nn}\mathfrak{d}) &= \delta_1(\mathcal{H}), \\ \{\delta_1(\mathcal{P}), \delta_1(\mathcal{Q})\} &\subset \{\delta_2(\mathcal{H}), \delta_3(\mathcal{H})\}, \\ \{\delta_1(\mathcal{R}), \mu_2(\mathcal{T}_h, \mathbf{nn}\mathfrak{d})\} &\subset \{\delta_4(\mathcal{H}), \delta_5(\mathcal{H}), \delta_6(\mathcal{H})\}. \end{cases}$$

We have the following proposition.

Proposition 3.9. *The first eigenvalues of $(\mathcal{H}, \mathfrak{d})$, satisfy the inequalities,*

$$(3.40) \quad \delta_1(\mathcal{H}) < \delta_2(\mathcal{H}) = \delta_3(\mathcal{H}) < \delta_4(\mathcal{H}) \leq \delta_5(\mathcal{H}) \leq \delta_6(\mathcal{H}) < \delta_7(\mathcal{H}).$$

More precisely,

- (1) *A first eigenfunction u_1 of $(\mathcal{H}, \mathfrak{d})$ arises from a first eigenfunction of $(\mathcal{R}, \mathbf{nn}\mathfrak{d})$. It also arises from a first eigenfunction of $(\mathcal{T}_h, \mathbf{nn}\mathfrak{d})$.*
- (2) *The eigenspace $\mathcal{E}(\delta_2)$ has dimension 2. It is generated by an eigenfunction u_2 arising from a first eigenfunction of $(\mathcal{P}, \mathfrak{d})$, and by an eigenfunction u_3 arising from a first eigenfunction of $(\mathcal{Q}, \mathfrak{d})$. These eigenfunctions also arise from first eigenfunctions of $(\mathcal{R}, \mathfrak{d}\mathbf{nn}\mathfrak{d})$ and $(\mathcal{R}, \mathbf{nn}\mathfrak{d}\mathfrak{d})$ respectively.*

- (3) The sum $\mathcal{E}(\delta_4(\mathcal{H})) \oplus \mathcal{E}(\delta_5(\mathcal{H})) \oplus \mathcal{E}(\delta_6(\mathcal{H}))$ has dimension 3. It is generated by eigenfunctions $\{u, v, w\}$, where u arises from a first eigenfunction of $(\mathcal{R}, \mathfrak{d}\mathfrak{d}\mathfrak{d})$, $v = T(u)$, and w arises from a second eigenfunction of $(\mathcal{T}_h, \mathfrak{n}\mathfrak{n}\mathfrak{d})$. The nodal set of w is a closed simple curve around the center of the hexagon.

Proof. We use the ideas of Subsection 2.2.

Assertion 1. The first Dirichlet eigenvalue is simple, and an associated eigenfunction u_1 does not change sign. A first eigenfunction must be invariant under all the symmetries D_i, M_j . This implies that u_1 arises from a first eigenfunction of $(\mathcal{R}, \mathfrak{n}\mathfrak{n}\mathfrak{d})$, and from a first eigenfunction of $(\mathcal{T}_h, \mathfrak{n}\mathfrak{n}\mathfrak{d})$.

Assertion 2. Let ψ be a first eigenfunction of $(\mathcal{Q}, \mathfrak{d})$. It does not change sign in \mathcal{Q} , and must be invariant with respect to M_2 . This means that it arises from a first eigenfunction of $(\mathcal{R}, \mathfrak{n}\mathfrak{d}\mathfrak{d})$. Extend ψ to u_3 on \mathcal{H} , so that it is anti-invariant under D_1 . The function u_3 is an eigenfunction of $(\mathcal{H}, \mathfrak{d})$. It is associated with $\delta_1(\mathcal{Q})$, belongs to $\mathcal{S}_{-,+}^0$, and its nodal set is $D_1 \cap \mathcal{H}$, so that $u_3 \notin \mathcal{S}_{-,+}^0$. Similarly, let θ be a first of $(\mathcal{P}, \mathfrak{d})$. It does not vanish in \mathcal{P} , and is invariant with respect to D_1 . It arises from a first eigenfunction of $(\mathcal{R}, \mathfrak{d}\mathfrak{n}\mathfrak{d})$, and can be extended to u_2 on \mathcal{H} , an eigenfunction of $(\mathcal{H}, \mathfrak{d})$, associated with $\delta_1(\mathcal{P})$, belonging to $\mathcal{S}_{+,-}^0$, and whose nodal set is $M_2 \cap \mathcal{H}$, so that $u_2 \notin \mathcal{S}_{+,-}^0$. Applying Lemma 3.2, and (3.39), we conclude that we can choose $u_3 = T(u_2)$, and hence that

$$(3.41) \quad \delta_2(\mathcal{H}) = \delta_3(\mathcal{H}) = \delta_1(\mathcal{P}) = \delta_1(\mathcal{Q}).$$

Assertion 3. We reason as in the proof of Assertion 2. From a first eigenfunction ϕ of $(\mathcal{R}, \mathfrak{d})$, we obtain an eigenfunction u of $(\mathcal{H}, \mathfrak{d})$, associated with $\delta_1(\mathcal{R})$, belonging to $\mathcal{S}_{-,-}^0$, whose nodal set is $(D_1 \cup M_2) \cap \mathcal{H}$. Then u does not belong to $\mathcal{S}_{-,-}^0$. Applying Lemma 3.2, and (3.39), we can choose $v = T(u)$. Using (3.39), more precisely the fact that $\mu_2(\mathcal{T}_h, \mathfrak{n}\mathfrak{n}\mathfrak{d}) \in \text{sp}(\mathcal{H}, \mathfrak{d})$, we now choose w to arise from a second eigenfunction ξ of $(\mathcal{T}_h, \mathfrak{n}\mathfrak{n}\mathfrak{d})$.

Because w is a Dirichlet eigenfunction of the convex set \mathcal{H} , the nodal set of w has the properties described in [1]. The function ξ has two nodal domains, and its nodal set must be a single simple line which is either closed inside \mathcal{T}_h , or goes from one side to another side (including the possibility to start or arrive at a vertex). Looking at all the possible configurations, we see that the function w would have at least seven nodal domains (this is prohibited by Courant's theorem), except in one case, when the nodal set of ξ is a curve from the open side of \mathcal{T}_h labelled 1, to the open side labelled 2. In this case, the function w has a closed nodal line and two nodal domains.

Note: We know that $\dim(\mathcal{E}(\delta_4) \oplus \mathcal{E}(\delta_5) \oplus \mathcal{E}(\delta_6)) = 3$. According to Remark 3.3, this implies that $(\mathcal{E}(\delta_4) \oplus \mathcal{E}(\delta_5) \oplus \mathcal{E}(\delta_6)) \cap \mathcal{S}^0 \neq \{0\}$.

The proposition is proved. \square

Remark 3.10. *We can determine which eigenvalues among the first four eigenvalues of $(\mathcal{R}, \mathbf{abd})$, $\mathbf{a}, \mathbf{b} \in \{\mathbf{d}, \mathbf{n}\}$, might possibly be $\delta_4(\mathcal{H})$. Table 3.5 takes Remark 3.7 and Assertions 1 and 2 into account. The word “no” in a cell means that the corresponding eigenvalue $\mu_i(\mathcal{R}, \mathbf{abd})$ cannot be equal to $\delta_4(\mathcal{H})$ due to the known inequalities on these eigenvalues. The only remaining possibilities are $\delta_4(\mathcal{H}) = \mu_2(\mathcal{R}, \mathbf{nn}\mathbf{d})$ (which might be a multiple eigenvalue), and $\delta_4(\mathcal{H}) = \mu_1(\mathcal{R}, \mathbf{d}\mathbf{d}\mathbf{d})$.*

TABLE 3.5. Possible choices for $\delta_4(\mathcal{H})$

$(\mathcal{R}, \mathbf{abd})$	μ_1	$<$	μ_2	\leq	μ_3	\leq	μ_4
$\mathbf{nn}\mathbf{d}$	$\delta_1(\mathcal{H})$	$<$		\leq		\leq	
	\wedge		\wedge		\wedge		\wedge
$\mathbf{d}\mathbf{nn}\mathbf{d}$	$\delta_2(\mathcal{H}) = \delta_3(\mathcal{H})$	$<$	no	\leq	no	\leq	no
$\mathbf{n}\mathbf{d}\mathbf{d}$	$\delta_2(\mathcal{H}) = \delta_3(\mathcal{H})$	$<$	no	\leq	no	\leq	no
	\wedge		\wedge		\wedge		\wedge
$\mathbf{d}\mathbf{d}\mathbf{d}$		$<$	no	\leq	no	\leq	no

3.4. Numerical results and $\mathbf{ECP}(\mathcal{H}, \mathbf{d})$. Using the numerical approximations given in Table 3.1, we infer the (numerical) lower bound $\delta_6(\mathcal{H}) > 35.17$. This implies that $\delta_6(\mathcal{H})$ is simple. It follows that u_6 arises from the second eigenfunction of \mathcal{T}_h , with mixed boundary condition $\mathbf{nn}\mathbf{d}$ (Dirichlet on the smaller side of \mathcal{T}_h , Neumann on the other sides). This provides the following numerical extension of Proposition 3.9,

Statement 3.11. *The Dirichlet eigenvalues of \mathcal{H} satisfy,*

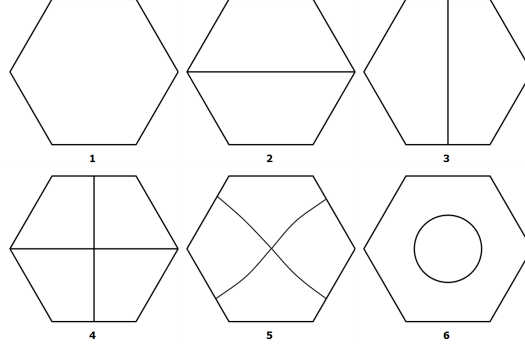
$$(3.42) \quad \delta_1(\mathcal{H}) < \delta_2(\mathcal{H}) = \delta_3(\mathcal{H}) < \delta_4(\mathcal{H}) = \delta_5(\mathcal{H}) < \delta_6(\mathcal{H}) < \delta_7(\mathcal{H}),$$

and

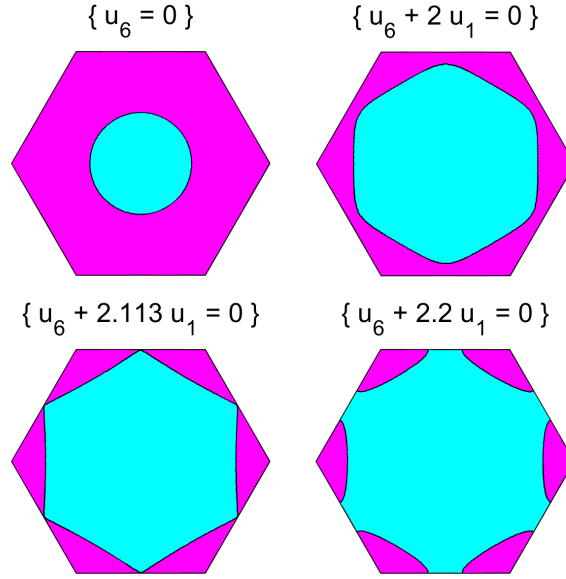
$$(3.43) \quad \delta_4(\mathcal{H}) = \delta_5(\mathcal{H}) = \delta_1(\mathcal{R}),$$

The eigenspace $\mathcal{E}(\delta_4)$ has dimension 2, and is generated by an eigenfunction u_4 which arises from the first eigenfunction of $(\mathcal{R}, \mathbf{d}\mathbf{d}\mathbf{d})$ and the function $u_5 = T(u_4)$. The eigenfunction u_6 associated with $\delta_6(\mathcal{H})$ arises from the second eigenfunction of $(\mathcal{T}_h, \mathbf{nn}\mathbf{d})$, and its nodal set is a simple closed curve enclosing the center of the hexagon.

Figure 3.8 displays the nodal patterns of first six Dirichlet eigenfunctions of \mathcal{H} .

FIGURE 3.8. $(\mathcal{H}, \mathfrak{d})$: nodal structure for the first six eigenfunctions

Plotting the nodal set of the linear combination $u_6 + a u_1$ for several values of a , one finds some values of a for which this function has 7 nodal domains, see Figure 3.9.

FIGURE 3.9. $(\mathcal{H}, \mathfrak{d})$: the ECP is false in $\mathcal{E}(\delta_1) \oplus \mathcal{E}(\delta_6)$

Statement 3.12. *Figure 3.9 provides a numerical evidence that the $\text{ECP}(\mathcal{H}, \mathfrak{d})$ is false.*

Remark 3.13. *For Statement 3.12, we do not really need to separate $\delta_6(\mathcal{H})$ from $\delta_5(\mathcal{H})$. It suffices to use Proposition 3.9, and more precisely the fact that there exists an eigenfunction in $\mathcal{E}(\delta_4) \oplus \mathcal{E}(\delta_5) \oplus \mathcal{E}(\delta_6)$, which arises from a second eigenfunction of $(\mathcal{T}_h, \mathbf{nn}\mathfrak{d})$. As in Subsection 2.6, we then need to know the nodal patterns in $\mathcal{E}(\mu_1(\mathcal{T}_h, \mathbf{nn}\mathfrak{d})) \oplus \mathcal{E}(\mu_2(\mathcal{T}_h, \mathbf{nn}\mathfrak{d}))$, or equivalently the nodal patterns in $\mathcal{E}(\mu_1(\mathcal{T}_e, \mathbf{nn}\mathfrak{d})) \oplus \mathcal{E}(\mu_2(\mathcal{T}_e, \mathbf{nn}\mathfrak{d}))$, see Remark 2.13 and Figure 2.8.*

3.5. Identification of the first Neumann eigenvalues of the regular hexagon.

3.5.1. *Numerical computations and preliminary remarks.* We did not find numerical computations of the Neumann eigenvalues of the hexagon in the literature. We use the same method as in Subsection 3.3.

Given an eigenspace $\mathcal{E}(\lambda)$ of $-\Delta$ for $(\mathcal{H}, \mathbf{n})$, we apply Lemma 3.2, and write

$$(3.44) \quad \mathcal{E}(\lambda) = \bigoplus_{\sigma, \tau \in \{+, -\}}^{\perp} \left(\mathcal{E}(\lambda) \cap \mathcal{S}_{\sigma, \tau}^0 \right) \bigoplus^{\perp} \left(\mathcal{E}(\lambda) \cap \mathcal{S}_{\sigma, \tau}^1 \right).$$

This means that to determine the eigenvalues of $(\mathcal{H}, \mathbf{n})$, it suffices to list the eigenvalues of $(\mathcal{R}, \mathbf{abn})$, with $\mathbf{a}, \mathbf{b} \in \{\mathfrak{d}, \mathbf{n}\}$, and to re-order them in non-decreasing order.

Table 3.6 displays the approximate values of the first four eigenvalues of $(\mathcal{R}, \mathbf{abn})$, as calculated by MATLAB.

TABLE 3.6. First four eigenvalues for $(\mathcal{R}, \mathbf{abn})$, $\mathbf{a}, \mathbf{b} \in \{\mathfrak{d}, \mathbf{n}\}$

$(\mathcal{R}, \mathbf{ab\mathfrak{d}})$	μ_1	$<$	μ_2	\leq	μ_3	\leq	μ_4
nnn	0	$<$	10.87	\leq	17.55	\leq	33.45
	\wedge		\wedge		\wedge		\wedge
\mathfrak{d}nn	4.04	$<$	17.55	\leq	32.91	\leq	49.90
	?		?		?		?
n\mathfrak{d}n	4.04	$<$	24.90	\leq	32.91	\leq	49.90
	\wedge		\wedge		\wedge		\wedge
\mathfrak{d}\mathfrak{d}n	10.87	$<$	33.45	\leq	54.77	\leq	71.71

Remark 3.14. *The following inequalities follow from Proposition 2.2, see [22],*

$$(3.45) \quad \begin{cases} \mu_i(\mathcal{R}, \mathbf{nnn}) < \mu_i(\mathcal{R}, \mathfrak{d}nn) < \mu_i(\mathcal{R}, \mathfrak{d}\mathfrak{d}n), \\ \mu_i(\mathcal{R}, \mathbf{nnn}) < \mu_i(\mathcal{R}, n\mathfrak{d}n) < \mu_i(\mathcal{R}, \mathfrak{d}\mathfrak{d}n). \end{cases}$$

These inequalities are indicated in Table 3.6 by the (rotated) strict inequality signs. The question marks indicate that one cannot compare the other values.

Eigenfunctions in $\mathcal{E}(\lambda) \cap \mathcal{S}_{\sigma, \tau}^0$ correspond to eigenfunctions of $-\Delta$ for $(\mathcal{T}_h, \mathbf{abn})$ with $\mathbf{a} = \mathfrak{d}$ (resp. $\mathbf{a} = \mathbf{n}$) if $\tau = -$ (resp. $\tau = +$), and similarly for \mathbf{b} , with σ . Table 3.7 displays the first non trivial eigenvalue of $(\mathcal{T}_h, \mathbf{abn})$.

Remarks 3.15. (1) *The first eigenvalue $\mu_1(\mathcal{T}_h, \mathbf{nnn})$ is 0. The second eigenvalue $\mu_2(\mathcal{T}_h, \mathbf{nnn})$ is also the second eigenvalue of an equilateral triangle with Neumann boundary condition. The corresponding eigenfunction has a nodal line which is a curve from side 1 to side 2 of \mathcal{T}_h .*

TABLE 3.7. Least non trivial eigenvalues for the hemiequilateral triangle

\mathcal{S}	$(\mathcal{T}_h, \mathbf{abn})$	Eigenvalue	Value
$\mathcal{S}_{+,+}^0$	$(\mathcal{T}_h, \mathbf{nnn})$	μ_2	$\mu_2 = \frac{16\pi^2}{9} \approx 17.55$
$\mathcal{S}_{+,-}^0$	$(\mathcal{T}_h, \mathbf{n\partial n})$	μ_1	$\mu_1 = \frac{16\pi^2}{9} \approx 17.55$
$\mathcal{S}_{-,+}^0$	$(\mathcal{T}_h, \mathbf{\partial nn})$	μ_1	$\mu_1 > \frac{4\pi^2}{\sqrt{3}} > 22.79$
$\mathcal{S}_{-,-}^0$	$(\mathcal{T}_h, \mathbf{\partial\partial n})$	μ_1	$\mu_1 > \frac{16\pi^2}{3} > 52.64$

(2) In the third line of Table 3.7, we use the fact that $\mu_1(\mathcal{T}_h, \mathbf{\partial nn})$ is the first Dirichlet eigenvalue of an equilateral rhombus. It is bounded from below by the first Dirichlet eigenvalue of a square with the same area (Pólya, see [19]).

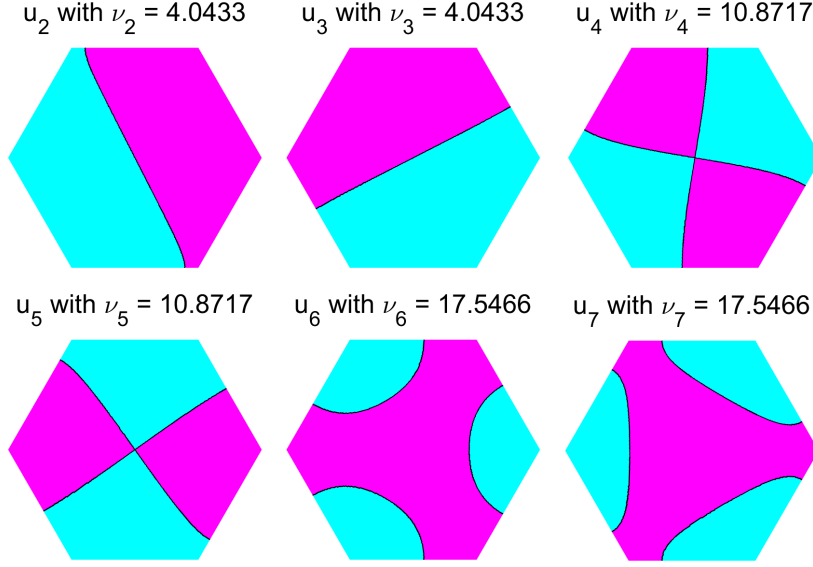
(3) In the fourth line of Table 3.7, we use the fact that $\mu_1(\mathcal{T}_h, \mathbf{\partial\partial n})$ is the first Dirichlet eigenvalue of an isosceles triangle with sides $(1, 1, \sqrt{3})$. It is bounded from below by the first Dirichlet eigenvalue of the equilateral triangle with the same area (Pólya, see [19]). Note that $\mu_1(\mathcal{T}_h, \mathbf{\partial\partial n}) > \mu_1(\mathcal{T}_h, \mathbf{\partial nn})$ according to Proposition 2.2.

One can also compute the eigenvalues of $(\mathcal{H}, \mathbf{n})$ directly, without taking the symmetries into account. The first Neumann eigenvalues of the hexagon are given in Table 3.8.

TABLE 3.8. First non-trivial Neumann eigenvalues of \mathcal{H}

Eigenvalue of \mathcal{H}	Approximation	Eigenvalue of \mathcal{R}
$\nu_2(\mathcal{H})$	≈ 4.04	$\mu_1(\mathcal{R}, \mathbf{\partial nn})$
$\nu_3(\mathcal{H})$	≈ 4.04	$\mu_1(\mathcal{R}, \mathbf{n\partial n})$
$\nu_4(\mathcal{H})$	≈ 10.87	$\mu_1(\mathcal{R}, \mathbf{\partial\partial n})$
$\nu_5(\mathcal{H})$	≈ 10.87	$\mu_2(\mathcal{R}, \mathbf{nnn})$
$\nu_6(\mathcal{H})$	≈ 17.55	$\mu_2(\mathcal{R}, \mathbf{\partial nn})$
$\nu_7(\mathcal{H})$	≈ 17.55	$\mu_3(\mathcal{R}, \mathbf{nnn})$
$\nu_8(\mathcal{H})$	≈ 24.90	$\mu_2(\mathcal{R}, \mathbf{n\partial n})$

Figure 3.10 displays the nodal patterns of eigenfunctions associated with the eigenvalues $\nu_i(\mathcal{H})$, $2 \leq i \leq 7$.

FIGURE 3.10. $(\mathcal{H}, \mathbf{n})$: nodal patterns $u_2 - u_7$

Remark 3.16. *The figures in Table 3.6 suggest that the Neumann eigenvalues of the hexagon come into well separated sets:*

$$\left\{ \begin{array}{ll} \nu_1(\mathcal{H}) &= 0, \\ \{\nu_2(\mathcal{H}), \nu_3(\mathcal{H})\} &\subset]3, 5[, \\ \{\nu_4(\mathcal{H}), \nu_5(\mathcal{H})\} &\subset]6, 14[, \\ \{\nu_6(\mathcal{H}), \nu_7(\mathcal{H})\} &\subset]15, 20[, \\ \nu_8(\mathcal{H}) &> 21. \end{array} \right.$$

In the following subsections, we analyze the possible eigenspaces and, more precisely, the double eigenvalues. Note that for Neumann eigenvalues we do not have monotonicity inequalities as the ones we used for Dirichlet eigenvalues in Subsection 3.3.2, so that we have to rely on the numerical evidence provided by Remark 3.16.

3.5.2. Analysis of the possible eigenspaces of $(\mathcal{H}, \mathbf{n})$. We divide the analysis into several steps.

Step 1: eigenvalue $\nu_1(\mathcal{H})$. The first Neumann eigenvalue is zero, and simple, with a corresponding eigenfunction u_1 which is constant. We have $u_1 \in \mathcal{S}_{+,+}^0$, and $\nu_1(\mathcal{H}) = \mu_1(\mathcal{T}_h, \mathbf{nnn})$.

Step 2: eigenvalue $\nu_2(\mathcal{H})$. Let $\mathcal{E}_2 = \mathcal{E}(\nu_2(\mathcal{H}))$ be the corresponding eigenspace.

◇ We claim that

$$(3.46) \quad \mathcal{E}_2 \cap \mathcal{S}^0 = \{0\}.$$

Indeed, Courant's nodal domain theorem and Lemma 3.2 imply that $\mathcal{E}_2 \cap \mathcal{S}_{\sigma,\tau}^0 = \{0\}$ unless $(\sigma, \tau) = (+, +)$. Assume that there exists some $0 \neq \phi \in \mathcal{E}_2 \cap \mathcal{S}_{+,+}^0$. The restriction of ϕ to \mathcal{T}_h would be an eigenfunction of $-\Delta$ for $(\mathcal{T}_h, \mathbf{nnn})$. Because $\nu_2(\mathcal{H})$ is the least non zero eigenvalue, we would have $\nu_2(\mathcal{H}) = \mu_2(\mathcal{T}_h, \mathbf{nnn})$, whose eigenfunction is known, with nodal set an arc from the side 1 to the side 2. The function ϕ would have a closed nodal line bounding a nodal domain strictly contained in the interior of \mathcal{H} , and we would have $\nu_2(\mathcal{H}) > \delta_1(\mathcal{H})$, contradicting the fact that $\nu_3(\mathcal{H}) \leq \delta_1(\mathcal{H})$ according to [21, Theorem 4.2].

As a by-product of (3.46), Lemma 3.2 tells us that the map T , defined by (3.22), is a bijection from \mathcal{E}_2 to \mathcal{E}_2 .

◇ We claim that

$$(3.47) \quad \mathcal{E}_2 \cap \mathcal{S}_{-,-}^1 = \{0\} \quad \text{and} \quad \mathcal{E}_2 \cap \mathcal{S}_{+,+}^1 = \{0\}.$$

The first assertion is clear by Courant's theorem. The second assertion follows from the fact that the map T is a bijection from $\mathcal{S}_{+,+}^1$ onto $\mathcal{S}_{-,-}^1$ which commutes with Δ .

◇ We claim that

$$(3.48) \quad \dim(\mathcal{E}_2 \cap \mathcal{S}_{+,-}^1) = \dim(\mathcal{E}_2 \cap \mathcal{S}_{-,+}^1) = 1,$$

and hence that $\text{mult}(\nu_2(\mathcal{H})) = 2$.

Indeed, using the map T again, we see that the spaces $\mathcal{E}_2 \cap \mathcal{S}_{+,-}^1$ and $\mathcal{E}_2 \cap \mathcal{S}_{-,+}^1$ have the same dimension. According to [15], see the statement p. 1170, line (-8), the multiplicity of $\nu_2(\mathcal{H})$ is less than or equal to 3, and we can conclude that this dimension must be 1. Here is an alternative argument for the case at hand. It suffices to prove that the dimension of \mathcal{E}_2 cannot be larger than or equal to 4. Indeed, assume that $\dim \mathcal{E}_2 \geq 4$. One could then find a point $x_0 \in \mathcal{H}$, and an eigenfunction $u_4 \in \mathcal{E}_2$ such that $u_4(x_0) \neq 0$. The subspace $\mathcal{E}_{2,x_0} = \{u \in \mathcal{E}_2 \mid u(x_0) = 0\}$ would have dimension 3, with a basis u_1, u_2, u_3 . The three vectors $\nabla u_1(x_0), \nabla u_2(x_0), \nabla u_3(x_0) \in \mathbb{R}^2$ would be linearly dependent, and we would then find a nontrivial $u \in \mathcal{E}_2$ such that $u(x_0) = \nabla u(x_0) = 0$. The nodal set of u would contain at least four semi-arcs emanating from x_0 , and we would reach a contradiction with the fact that u has only two nodal domains by Courant's theorem.

Because $\mu_2(\mathcal{R}, \mathbf{nnn})$ is an eigenvalue of $(\mathcal{H}, \mathbf{n})$, we have proved the following lemma.

Lemma 3.17. *The eigenvalue $\nu_2(\mathcal{H})$ has multiplicity 2,*

$$(3.49) \quad \nu_2(\mathcal{H}) = \mu_1(\mathcal{R}, \mathbf{dnn}) = \mu_1(\mathcal{R}, \mathbf{ndn}),$$

and corresponding eigenfunctions u_2, u_3 arise from the first eigenfunctions of $-\Delta$ for $(\mathcal{R}, \mathbf{dnn})$ and $(\mathcal{R}, \mathbf{ndn})$. Furthermore,

$$\nu_2(\mathcal{H}) = \nu_3(\mathcal{H}) < \mu_2(\mathcal{R}, \mathbf{nnn}).$$

Step 3: eigenvalue $\nu_4(\mathcal{H})$. Let $\mathcal{E}_4 = \mathcal{E}(\nu_4(\mathcal{H}))$ be the eigenspace associated with the eigenvalue $\nu_2(\mathcal{H})$.

◇ We claim that

$$(3.50) \quad \mathcal{E}_4 \cap \mathcal{S}^0 = \{0\}.$$

Indeed, by Courant's theorem and Lemma 3.2,

$$(3.51) \quad \mathcal{E}_4 \cap \mathcal{S}_{\sigma,\tau}^0 = \{0\},$$

unless $(\sigma, \tau) = (+, +)$. Assume that there exists some $0 \neq \phi \in \mathcal{S}_{+,+}^0$. Then, we would have $\nu_4(\mathcal{H}) = \mu_2(\mathcal{T}_h, \mathbf{nnn}) = \frac{16\pi^2}{9}$. Observe that $\nu_2(\mathcal{T}_e) = \mu_2(\mathcal{T}_h, \mathbf{nnn}) = \mu_1(\mathcal{T}_h, \mathbf{n\partial n})$. This means that \mathcal{E}_4 would also contain a function in $\mathcal{S}_{+,-}^0$ having 6 nodal domains which would contradict Courant's theorem.

From (3.50) and Proposition 2.3 ([25, Theorem 1.1]), we deduce that

$$(3.52) \quad \nu_4 < \mu_2(\mathcal{T}_h, \mathbf{nnn}) = \mu_1(\mathcal{T}_h, \mathbf{n\partial n}) < \mu_1(\mathcal{T}_h, \mathbf{\partial nn}) < \mu_1(\mathcal{T}_h, \mathbf{\partial\partial n}).$$

◇ We claim that

$$(3.53) \quad \mathcal{E}_4 \cap \mathcal{S}_{+,-}^1 = \{0\} \text{ and } \mathcal{E}_4 \cap \mathcal{S}_{-,+}^1 = \{0\}.$$

Indeed, assume that $\mathcal{E}_4 \cap \mathcal{S}_{+,-}^1 \neq \{0\}$ or, equivalently using the map T , that $\mathcal{E}_4 \cap \mathcal{S}_{-,+}^1 \neq \{0\}$. Then, we would have

$$(3.54) \quad \nu_4 = \mu_2(\mathcal{R}, \mathbf{n\partial n}) = \mu_2(\mathcal{R}, \mathbf{\partial nn}).$$

These eigenvalues are strictly larger than $\mu_2(\mathcal{R}, \mathbf{nnn})$ by (3.45), and this would contradict the fact that $\nu_3(\mathcal{H}) < \mu_2(\mathcal{R}, \mathbf{nnn})$, see Step 2, because $\mu_2(\mathcal{R}, \mathbf{nnn})$ is an eigenvalue for $(\mathcal{H}, \mathbf{n})$.

As a by-product, we have the inequalities

$$(3.55) \quad \begin{cases} \nu_4 < \mu_2(\mathcal{R}, \mathbf{\partial nn}) < \mu_2(\mathcal{R}, \mathbf{\partial\partial n}), \\ \nu_4 < \mu_2(\mathcal{R}, \mathbf{n\partial n}) < \mu_2(\mathcal{R}, \mathbf{\partial\partial n}). \end{cases}$$

◇ It follows from the above arguments that we must have,

$$(3.56) \quad \dim(E_4 \cap \mathcal{S}_{-,-}^1) = \dim(E_4 \cap \mathcal{S}_{+,+}^1) > 0,$$

and hence that $\dim \mathcal{E}_4 \geq 2$, so that $\nu_4(\mathcal{H}) = \nu_5(\mathcal{H}) = \mu_1(\mathcal{R}, \mathbf{\partial\partial n}) = \mu_2(\mathcal{R}, \mathbf{nnn})$, with corresponding eigenfunction u_4, u_5 for $(\mathcal{H}, \mathbf{n})$.

Remark 3.18. According to Table 3.6 and Remark 3.16, $\dim \mathcal{E}_4 = 2$.

Step 4: eigenvalue $\nu_6(\mathcal{H})$. So far, we have established the following facts

$$\nu_1(\mathcal{H}) < \nu_2(\mathcal{H}) = \nu_3(\mathcal{H}) < \nu_4(\mathcal{H}) = \nu_5(\mathcal{H}) \leq \dots$$

or

$$\mu_1(\mathcal{R}, \mathbf{nnn}) < \mu_1(\mathcal{R}, \mathbf{\partial nn}) = \mu_1(\mathcal{R}, \mathbf{n\partial n}) < \mu_2(\mathcal{R}, \mathbf{nnn}) = \mu_1(\mathcal{R}, \mathbf{\partial\partial n}).$$

The next eigenvalue $\nu_6(\mathcal{H})$ should belong to the set,

$$(3.57) \quad \{\mu_2(\mathcal{R}, \mathbf{\partial nn}), \mu_2(\mathcal{R}, \mathbf{n\partial n}), \mu_2(\mathcal{R}, \mathbf{\partial\partial n}), \mu_3(\mathcal{R}, \mathbf{nnn})\}$$

We can exclude $\mu_2(\mathcal{R}, \mathfrak{d}\mathfrak{d}\mathfrak{n})$ because it is larger than both $\mu_2(\mathcal{R}, \mathfrak{d}\mathfrak{n}\mathfrak{n})$ and $\mu_2(\mathcal{R}, \mathfrak{n}\mathfrak{d}\mathfrak{n})$ according to (3.45) ([22, Proposition 2.3]).

The eigenvalues of $(\mathcal{T}_h, \mathfrak{a}\mathfrak{b}\mathfrak{n})$, $\mathfrak{a}, \mathfrak{b} \in \{\mathfrak{d}, \mathfrak{n}\}$, are eigenvalues of $(\mathcal{H}, \mathfrak{n})$. Using Table 3.7 and Remark 3.16, we can conclude that

$$(3.58) \quad \nu_6(\mathcal{H}) = \nu_7(\mathcal{H}) = \mu_1(\mathcal{T}_h, \mathfrak{n}\mathfrak{d}\mathfrak{n}) = \mu_2(\mathcal{T}_h, \mathfrak{n}\mathfrak{n}\mathfrak{n}),$$

and that associated eigenfunctions u_6, u_7 arise from the first and second eigenfunctions of $(\mathcal{T}_h, \mathfrak{n}\mathfrak{d}\mathfrak{n})$.

Statement 3.19. *From the numerical evidence in Remark 3.16, we conclude that $\nu_i(\mathcal{H})$ have multiplicity 2 for $i \in \{2, 4, 6\}$, and that $\nu_6(\mathcal{H})$ and $\nu_7(\mathcal{H})$ arise from eigenvalues of $(\mathcal{T}_h, \mathfrak{a}\mathfrak{b}\mathfrak{n})$.*

3.6. Numerical computations and $\text{ECP}(\mathcal{H}, \mathfrak{n})$. The first Neumann eigenvalue of the hexagon, $\nu_1(\mathcal{H})$, is 0, with associated eigenfunction $u_1 \equiv 1$. As sixth Neumann eigenfunction u_6 of the hexagon, we can choose the function which arises from an eigenfunction for $\mu_2(\mathcal{T}_h, \mathfrak{n}\mathfrak{n}\mathfrak{n})$, or equivalently from a D -invariant second eigenfunction ψ of $(\mathcal{T}_e, \mathfrak{n})$. It follows from [9, Section 3] that $\text{ECP}(\mathcal{T}_e, \mathfrak{n})$ is false, i.e., that there exists some real value a such that $\psi + a$ has three nodal domains in \mathcal{T}_e . It follows that $u_6 + a$ has seven nodal domains, so that $\text{ECP}(\mathcal{H}, \mathfrak{n})$ is false.

Alternatively, we can look at $\mu_3(\mathcal{R}, \mathfrak{n}\mathfrak{n}\mathfrak{n}) = \mu_2(\mathcal{T}_h, \mathfrak{n}\mathfrak{n}\mathfrak{n})$. Figure 3.11 displays the nodal pattern and the level lines of an eigenfunction for $\mu_3(\mathcal{R}, \mathfrak{n}\mathfrak{n}\mathfrak{n})$. By reflection with respect to the lines D_1 and M_2 , one obtains a Neumann eigenfunction $u_{\mathcal{H}}$ of \mathcal{H} , associated with $\nu_6(\mathcal{H}) = \nu_7(\mathcal{H})$, whose nodal set is a closed simple curve around O , and whose level lines are displayed in Figure 3.12; some level lines of $u_{\mathcal{H}}$ have six connected components, one component near each vertex of the hexagon, so that $\text{ECP}(\mathcal{H}, \mathfrak{n})$ is false.

Statement 3.20. *The $\text{ECP}(\mathcal{H}, \mathfrak{n})$ is false in $\mathcal{E}(\nu_1) \oplus \mathcal{E}(\nu_6)$.*

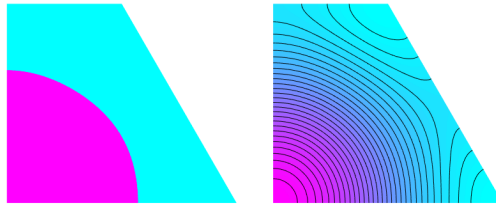
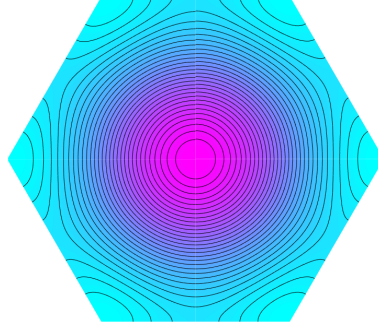


FIGURE 3.11. $(\mathcal{R}, \mathfrak{n}\mathfrak{n}\mathfrak{n})$: nodal set and level lines for u_3

FIGURE 3.12. Level lines of $u_{\mathcal{H}}$

4. FINAL COMMENTS

4.1. Numerical computations. In Subsection 3.6, we used numerical approximations of the first eigenvalues of the problems $(\mathcal{R}, \mathbf{a}\mathbf{b}\mathbf{b})$ and $(\mathcal{T}_h, \mathbf{a}\mathbf{b}\mathbf{n})$ in order to identify the first eight eigenvalues of $(\mathcal{H}, \mathbf{n})$, and to conclude that $\text{ECP}(\mathcal{H}, \mathbf{n})$ is false (we also used the fact that some eigenfunctions are known explicitly), see Table 4.1.

	R-nnn	R-dnn	R-ndn	R-ddn	H-Neumann
μ_1	0,00000	4,04324	4,04324	10,87153	0,00000
μ_2	10,87154	17,54612	24,89890	33,44806	4,04327
μ_3	17,54612	32,91475	32,91476	54,77365	4,04327
μ_4	33,44804	49,90025	49,90023	71,71384	10,87171
μ_5	52,63932	70,18634	80,45178	95,73076	10,87172
μ_6	54,77368	80,45171	83,83234	111,78681	17,54658
μ_7	70,18642	96,57468	96,57456	128,35718	17,54660
μ_8	95,73076	122,82951	130,09479	159,56644	24,89989

TABLE 4.1. Neumann eigenvalues of \mathcal{H}

We did not find tables providing the first eigenvalues of $(\mathcal{H}, \mathbf{n})$ in the literature. We used the symmetries, and computed the eigenvalues of the problems $(\mathcal{R}, \mathbf{a}\mathbf{b}\mathbf{n})$ and $(\mathcal{T}_h, \mathbf{a}\mathbf{b}\mathbf{n})$ with MATLAB. We checked the accuracy of our computations in two ways.

- (1) First, using the symmetries, we computed the eigenvalues of $(\mathcal{R}, \mathbf{a}\mathbf{b}\mathbf{d})$ and $(\mathcal{T}_h, \mathbf{a}\mathbf{b}\mathbf{d})$ in order to obtain the Dirichlet eigenvalues of the hexagon. We then compared the results with the tables in [13], see Table 4.2.
- (2) Second, we computed the eigenvalues of $(\mathcal{T}_h, \mathbf{a}\mathbf{b}\mathbf{c})$, and compared the results both with explicitly known eigenvalues, and with the tables in [16], see Tables 4.3 and 4.4.

Remark 4.1. *The tables in [13, 16] are organized according to the symmetries, and they provide the square roots of the eigenvalues. In [16], the labelling of the sides of \mathcal{T}_h is different from ours: we use*

	R-nnd	R-dnd	R-ndd	R-ddd	H-Dirichlet	CurKut1999
μ_1	7,15537	18,13185	18,13186	32,45236	7,15545	7,15534
μ_2	32,45240	47,63049	52,63929	70,14278	18,13234	18,13168
μ_3	37,49207	60,10698	60,10704	87,53571	18,13236	18,13168
μ_4	70,14288	94,33006	94,32994	122,82902	32,45398	32,45186
μ_5	87,53590	110,36078	122,82935	145,49250	32,45400	32,45186
μ_6	90,06261	125,05361	125,05369	165,52862	37,49405	37,49136
μ_7	120,87511	152,67570	152,67575	187,35944	47,63410	47,62937
μ_8	145,49213	183,45321	183,45364	228,12299	52,64351	52,63789

TABLE 4.2. Dirichlet eigenvalues of \mathcal{H}

Dirichlet		N	N x 16 π^2 /9	ML- μ	Jones93- μ -LR
nnd-oe	μ_1			7,15536	7,15568
nnd-oe	μ_2			37,49188	37,49395
nnd-oe	μ_3			90,06160	90,07301
nnd-oe	μ_4			120,87283	120,88563
ndd-oe	μ_1			47,63020	47,63622
ndd-oe	μ_2			110,35921	110,38024
ndd-oe	μ_3			189,52747	189,60464
ndd-oe	μ_4			224,69274	224,68511
dnd-oe	μ_1	3	52,63789	52,63891	52,63793
dnd-oe	μ_2	7	122,82174	122,82735	122,82181
dnd-oe	μ_3	12	210,55156	210,56758	210,55171
dnd-oe	μ_4	13	228,09752	228,11669	228,09759
ddd-oo	μ_1	7	122,82174	122,82707	122,82181
ddd-oo	μ_2	13	228,09752	228,11639	228,09759
ddd-oo	μ_3	19	333,37330	333,41196	333,37282
ddd-oo	μ_4	21	368,46523	368,51464	368,46338

TABLE 4.3. Eigenvalues of \mathcal{T}_h (Dirichlet on shortest side)

$\mathfrak{d}, \mathfrak{n}$ to indicate the boundary condition on each side, while Jones uses the notation e, o (for even and odd). For the reader's convenience, we indicate both labellings in the first column of Tables 4.3 and 4.4. The fourth column of each table contains the eigenvalues which are known explicitly; the fifth column contains our computations. The sixth column of each table contains the values deduced from [16], Tables 7–14.

Remark 4.2. Our purpose in this paper is to identify eigenvalues, and their relations with the symmetries, not to find high precision approximations as in [16, 17]. The approximated values which appear in the tables indicate that the approximations are indeed sufficient to identify the eigenvalues (because we took the symmetries into consideration from the start, and identified multiple eigenvalues).

Neumann		N	$N \times 16\pi^2/9$	ML- μ	Jones93- μ -LR
nnn-eee	μ_1	0	0,00000	0,00000	0,00000
nnn-eee	μ_2	1	17,54596	17,54608	17,54596
nnn-eee	μ_3	3	52,63789	52,63891	52,63793
nnn-eee	μ_4	4	70,18385	70,18573	70,18385
ndn-eoe	μ_1	1	17,54596	17,54608	17,54596
ndn-eoe	μ_2	4	70,18385	70,18561	70,18385
ndn-eoe	μ_3	7	122,82174	122,82718	122,82181
ndn-eoe	μ_4	9	157,91367	157,92305	157,91441
dnn-eeo	μ_1			24,89880	24,90489
dnn-eeo	μ_2			83,83145	83,83966
dnn-eeo	μ_3			140,45719	140,61691
dnn-eeo	μ_4			169,23939	169,22888
ddn-ooo	μ_1			71,71299	71,74751
ddn-ooo	μ_2			169,78103	169,84084
ddn-ooo	μ_3			234,07541	234,37467
ddn-ooo	μ_4			292,73528	292,71446

TABLE 4.4. Eigenvalues of \mathcal{T}_h (Neumann on shortest side)

In Subsections 2.5 and 3.4, we also used numerical approximations of the first and second eigenfunctions of $(\mathcal{T}_h, \mathbf{nn}\mathbf{d})$ in order to show that the ECP($\mathcal{R}h_e, \mathbf{n}$) is false in $\mathcal{E}(\nu_2) \oplus \mathcal{E}(\nu_5)$, and that ECP(\mathcal{H}, \mathbf{d}) is false in $\mathcal{E}(\delta_1) \oplus \mathcal{E}(\delta_6)$.

4.2. Final remarks.

4.2.1. The estimates in Table 3.3 are valid for the regular polygon \mathcal{P}_n with n sides, inscribed in the circle of radius 1. The upper bounds get better when n increases, and for $n \geq 9$, they are sufficient to separate $\delta_6(\mathcal{P}_n)$ from $\delta_5(\mathcal{P}_n)$. This shows that $\delta_6(\mathcal{P}_n)$ is a simple eigenvalue for $n \geq 6$, and that an associated eigenfunction u_6 arises from the first eigenfunction of a right triangle with smallest angle $\frac{\pi}{n}$, hypotenuse of length 1, with Dirichlet condition on the smallest side and Neumann condition on the other sides. Equivalently, the eigenfunction u_6 arises from a first eigenfunction of an isosceles triangle whose apex angle is $\frac{2\pi}{n}$, with equal sides of length 1, Dirichlet condition on the smallest side and Neumann condition on the equal sides. Note that $\delta_6(\mathcal{D})$ corresponds to the second radial eigenfunction of the disc.

4.2.2. Based on our computations, we conjecture that the ECP($\mathcal{P}_n, \mathbf{a}$) is false for any regular polygon $\mathcal{P}_n \subset \mathbb{R}^2$ with $n \geq 6$ sides, and $\mathbf{a} \in \{\mathbf{d}, \mathbf{n}\}$, with some linear combination $u_6 + au_1$ of a sixth and a first eigenfunctions providing a counterexample with $(n+1)$ nodal domains. Using [23, Theorem B], one can show that ECP($\mathcal{P}_n, \mathbf{n}$) is false for n sufficiently large, see [6]. The simulations show that the first six

Dirichlet eigenfunctions of \mathcal{P}_n look very much like the first six Dirichlet eigenfunctions of the disk \mathcal{D} .

4.2.3. The above considerations do not provide any counter-example to the ECP when the number of sides is 4 or 5. It is not clear whether the ECP is false for the square and for the regular pentagon. It is not clear either whether the ECP is false for the disk.

4.2.4. In the Neumann case, the present paper is also relevant to the investigation of the level lines of Neumann eigenfunctions. Such investigations arise when studying the hot spots conjecture.

REFERENCES

- [1] G. Alessandrini. Nodal lines of eigenfunctions of the fixed membrane problem in general convex domains. *Comment. Math. Helvetici* 69 (1994) 142–154. [27](#)
- [2] V. Arnold. The topology of real algebraic curves (the works of Petrovskii and their development). *Uspekhi Math. Nauk.* 28:5 (1973) 260–262. English translation in [4]. [3](#)
- [3] V. Arnold. Topological properties of eigenoscillations in mathematical physics. *Proceedings of the Steklov Institute of Mathematics* 273 (2011) 25–34. [3](#)
- [4] V. Arnold. *Topology of real algebraic curves (Works of I.G. Petrovskii and their development)*. Translated by Oleg Viro. In *Collected works, Volume II. Hydrodynamics, Bifurcation theory and Algebraic geometry, 1965–1972*. Edited by A.B. Givental, B.A. Khesin, A.N. Varchenko, V.A. Vassilev, O.Ya. Viro. Springer 2014. [3](#), [39](#)
- [5] L. Bauer and E.L. Reiss. Cutoff Wavenumbers and Modes of Hexagonal Waveguides. *SIAM Journal on Applied Mathematics* 35:3 (1978) 508–514. [23](#)
- [6] P. Bérard, P. Charron and B. Helffer. Non-boundedness of the number of nodal domains of a sum of eigenfunctions. *arXiv:1906.03668*. [38](#)
- [7] P. Bérard and B. Helffer. Nodal sets of eigenfunctions, Antonie Stern’s results revisited. *Séminaire de théorie spectrale et géométrie (Grenoble)* 32 (2014–2015) 1–37. http://tsg.cedram.org/item?id=TSG_2014-2015__32__1_0. [2](#)
- [8] P. Bérard and B. Helffer. Courant-sharp eigenvalues for the equilateral torus, and for the equilateral triangle. *Letters in Math. Physics* 106 (2016) 1729–1789. [8](#)
- [9] P. Bérard and B. Helffer. On Courant’s nodal domain property for linear combinations of eigenfunctions, Part I. *Documenta Mathematica* 23 (2018) 1561–1585. *arXiv:1705.03731*. [3](#), [8](#), [12](#), [15](#), [35](#)
- [10] P. Bérard and B. Helffer. Sturm’s theorem on zeros of linear combinations of eigenfunctions. *Expositiones Mathematicae*, in press. DOI <https://doi.org/10.1016/j.exmath.2018.10.002>. *arXiv:1706.08247* (expanded version). [2](#)
- [11] P. Bérard and B. Helffer. Level sets of certain Neumann eigenfunctions under deformation of Lipschitz domains. Application to the Extended Courant Property. To appear in *Annales de la Faculté des Sciences de Toulouse*. <http://afst.cedram.org/>. *arXiv:1805.01335*. [3](#)
- [12] R. Courant and D. Hilbert. *Methods of mathematical physics. Vol. 1. First English edition*. Interscience, New York 1953. [2](#)
- [13] L.M. Cureton and J.R. Kuttler. Eigenvalues of the Laplacian on regular polygons and polygons resulting from their dissection. *Journal of Sound and Vibration* 220:1 (1999) 83–98. [23](#), [36](#)

- [14] G. Gladwell and H. Zhu. The Courant-Herrmann conjecture. *ZAMM-Z. Angew. Math. Mech.* 83:4 (2003) 275–281. [3](#)
- [15] T. Hoffmann-Ostenhof, P. Michor and N. Nadirashvili. Bounds on the multiplicities of eigenvalues for fixed membranes. *GAFA, Geom. Func. Anal.* 9 (1999) 1169–1188. [33](#)
- [16] R.S. Jones. The one-dimensional three-body problem and selected wave-guide problems: solutions of the two-dimensional Helmholtz equation. PhD Thesis, The Ohio State University, 1993. Retyped 2004, available at <http://www.hbelabs.com/phd/>. [23](#), [36](#), [37](#)
- [17] R.S. Jones. Computing ultra-precise eigenvalues of the Laplacian with polygons. *Adv. Comput. Math.* 43 (2017) 1325–1354. arXiv:1602.08636v1. [23](#), [37](#)
- [18] N. Kuznetsov. On delusive nodal sets of free oscillations. *Newsletter of the European Mathematical Society* 96 (2015) 34–40. [3](#)
- [19] R. Laugesen and B. Siudeja. Triangles and other special domains. Chapter 1 in *Shape optimization and spectral theory*. A. Henrot, ed. De Gruyter, Berlin 2017. [24](#), [31](#)
- [20] C. Léna. Pleijel’s nodal domain theorem for Neumann and Robin eigenfunctions. *Annales de l’institut Fourier* 69:1 (2019) 283–301. arXiv:1609.02331. [2](#)
- [21] H. Levine and H. Weinberger. Inequalities between Dirichlet and Neumann eigenvalues. *Arch. Rational Mech. Anal.* 94 (1986) 193–208. [33](#)
- [22] V. Lotoreichik and J. Rohleder. Eigenvalue inequalities for the Laplacian with mixed boundary conditions. *J. Differential Equations* 263 (2017) 491–508. [7](#), [10](#), [23](#), [30](#), [35](#)
- [23] Y. Miyamoto. A planar convex domain with many isolated “hot spots” on the boundary. *Japan J. Indust. Appl. Math.* 30 (2013) 145–164. [38](#)
- [24] Å. Pleijel. Remarks on Courant’s nodal theorem. *Comm. Pure. Appl. Math.* 9 (1956) 543–550. [2](#), [3](#)
- [25] B. Siudeja. On mixed Dirichlet-Neumann eigenvalues of triangles. *Proc. Amer. Math. Soc.* 144 (2016) 2479–2493. [8](#), [10](#), [11](#), [34](#)
- [26] O. Viro. Construction of multi-component real algebraic surfaces. *Soviet Math. dokl.* 20:5 (1979) 991–995. [3](#)

PB: UNIVERSITÉ GRENOBLE ALPES AND CNRS, INSTITUT FOURIER, CS 40700, 38058 GRENOBLE CEDEX 9, FRANCE.

E-mail address: pierreherberard@gmail.com

BH: LABORATOIRE JEAN LERAY, UNIVERSITÉ DE NANTES AND CNRS, F44322 NANTES CEDEX, FRANCE, AND LMO, UNIVERSITÉ PARIS-SUD.

E-mail address: Bernard.Helffer@univ-nantes.fr